




## Impact Stiffness of Linear Viscoelastic Model for Seismic Pounding Simulation: An Experimental Evaluation

Yazan Jaradat <sup>1\*</sup>, Harry Far <sup>1</sup> 

<sup>1</sup> School of Civil and Environmental Engineering, Faculty of Engineering and Information Technology, University of Technology Sydney (UTS), Australia.

Received 15 March 2023; Revised 20 May 2023; Accepted 26 May 2023; Published 01 June 2023

### Abstract

Pounding between adjacent structures occurs when the separating distance within the two buildings is inadequate to contain the movement between them during an earthquake event. Seismic pounding can lead to significant harm or even the destruction of neighbouring structures. In creating a model for structural response, impact stiffness is considered as a critical factor in calculating the impact force throughout the collision within adjacent structures. It is important to derive realistic stiffness values when performing a numerical simulation of pounding forces within abutting structures to attain valid results. The objective of this study is to ascertain the impact stiffness within the linear viscoelastic contact model, using data obtained from shaking table experiments of pounding between neighboring five-storey and 15-storey single-bay model of steel-frame. The steel models were subjected to scaled ground acceleration records, two far-field and two near-field. The study's findings indicate that there is a significant discrepancy between the theoretical impact parameters and the measured experimental value because the assumptions made to derive the theoretical formulas do not align with the actual impact conditions. The accuracy and precision of the experimental formula adopted in this study have been validated in comparison with the numerical results.

**Keywords:** Seismic Pounding; Steel Structure; Impact Stiffness Parameter; Shake Table Test; Linear Viscoelastic Model; Impact Force; Seismic Response; Seismic Performance.

## 1. Introduction

One of the significant risks for adjacent structures during earthquakes is the pounding that can occur between them. This phenomenon is attributed to the fact that adjacent buildings or bridge elements with varying dynamic properties tremble out of phase as a result of restricted or deficient separation distance to support the relative displacement. Adjoining structures with insufficient spacing are conceived as loose structures without taking into account the pounding effect during earthquake loading. Neglect can lead to the failure of structures. Seismic pounding causes soaring magnitudes and brief interval acceleration pulses that could induce slight non-structural damage or serious structural damage such as the partial or total collapse of buildings and bridges [1–3]. Hence, a determination of the seismic pounding hazard is imperative in order to come up with future calibrations of the seismic designs of adjacent structures.

Several earthquakes have induced well-documented incidents of structural pounding resulting from seismic activity. According to several researchers [4–7], one of the most destructive examples of damage caused by seismic pounding occurred throughout the earthquake that hit Mexico City in 1985. Approximately 15% of the buildings that were affected by this earthquake were damaged or collapsed due to the pounding, and in 20–30% of cases, the impact between adjacent buildings was identified as a significant contributing factor to the damage or collapse of the structures. Investigations of

\* Corresponding author: [yazan.jaradat@student.uts.edu.au](mailto:yazan.jaradat@student.uts.edu.au)

 <http://dx.doi.org/10.28991/CEJ-2023-09-06-01>



© 2023 by the authors. Licensee C.E.J, Tehran, Iran. This article is an open access article distributed under the terms and conditions of the Creative Commons Attribution (CC-BY) license (<http://creativecommons.org/licenses/by/4.0/>).

pounding damage between adjacent structures were conducted based on past and present earthquakes. Pounding damage was acknowledged in numerous extreme earthquakes, such as the 1999 Taiwan Chi-Chi earthquake [8], and the 2008 Wenchuan earthquake [9]. After the 2011 Christchurch earthquake, pounding incidents between neighbouring buildings as well as bridge structures were observed and reported [10, 11]. In the 2015 Gorkha earthquake in Nepal, the pounding events noticed in valley settlements were limited to multistorey reinforced concrete structures, while those observed at hilly urban settlements were focused on masonry structures [12].

Numerous studies have been implemented to explore the effects of seismic pounding between reinforced concrete buildings situated in close proximity [13–15], the pounding of adjoining steel-frame structures [16–18], the pounding of adjacent structures taking into account soil-structure interaction [19–21], and the pounding of a bridge deck excited under earthquake acceleration [22, 23]. There are two common types of typically classified pounding scenarios: floor-to-floor (slab-to-slab) impact and floor-to-column (slab-to-column) impact [24]. The scenario where the crashing structures have the same floor heights is known as slab-to-slab collision, whereas slab-to-column collision is obvious when the floor heights of the colliding edifices are unequal. Because of the substantial shear forces applied to the middle section of struck columns, it is evident that slab-to-column pounding is more serious than slab-to-slab pounding [5].

Structural seismic pounding is an extreme, nonlinear occurrence. It encompasses plastic bending, crushing, local cracking, and rupturing, along with friction destruction at the contact area. Taking into consideration the complexity of this phenomenon, performing precise mathematical analysis can be challenging for this type of concern. Therefore, using assumptions as a basis for analysis, various contact models were created to investigate and analyse structural pounding during a seismic activity like an earthquake. The models include the linear spring model [16, 25], the linear viscoelastic model [26–29], the nonlinear elastic model [17, 30, 31], the Hertz-damp model [32, 33], and the nonlinear viscoelastic model [3, 31, 34]. The limitation of the linear spring model along with the Hertz model is that they assume full elasticity and do not consider the dissipated energy due to damping. This can result in inaccurate predictions of impact forces and structural response during pounding. The other impact models, namely, the linear viscoelastic, Hertz-damp, in addition to nonlinear viscoelastic models, were discovered to provide relatively accurate outcomes for overall structural reaction as long as the factors in these three impact models are well chosen [32].

The linear viscoelastic model is commonly adopted in the simulation of structural induced pounding for the reason that of its simplicity, which can easily be applied in most commercial computer codes or software programs, as revealed by most researchers [4, 31, 35–37]. The model has a significant limitation related to the negative impact force detected just prior to the separation of two colliding structures. This phenomenon is not physically described, and it is attributed to the fact that the linear damping term of the model is active during the entire contact period, assuming uniform energy dissipation [38]. In order to correct the weakness of the linear viscoelastic model, Komodromos et al. [39] recommended a variation. The proposed variation also has a significant constraint: the correct value of the impact stiffness  $k$  to be applied in the simulation could not be determined beforehand. Licari et al. [40] recommended a special "viscoelastic multi-link" finite element contact model for seismic driving between multistorey reinforced concrete frame edifices. The proposed model was designed to replicate the nonlinear, time-dependent damping coefficients. Guo et al. [41] conducted shaking table tests on a highway bridge model made from steel to evaluate the impact stiffness of four classes of contact-element models. The study's findings suggest that the theoretical impact variables considerably surpass the values determined through experimentation since the assumptions made to develop the models do not align with the actual impact conditions. An impact spring with under-stiffness can result in the overlaying of adjacent structures. Alternatively, using a spring with an extremely high stiffness value can result in unrealistic, excessively large lateral impact forces, which can introduce numerical instabilities and convergence issues.

Several studies have shown that impact stiffness  $k$  has a great bearing on the pounding response, particularly on the inertia force response and the structural acceleration response, though the researchers have proposed various methods and equations to compute the stiffness of the impact element model [26, 42–46]. The decision to employ impact stiffness when examining structural pounding is difficult as it necessitates taking into account the uncertainties in the shapes of the impact surfaces, the material properties when subjected to impact loads, the fluctuating impact velocities, and additional factors. There is scant research on choosing impact stiffness. Usually, in the linear viscoelastic model, the axial stiffness of the colliding elements is used as a basis to assume proportionality with the impact stiffness. This method is usually adopted in evaluating structural seismic pounding [32].

The axial stiffness of a girder is used as the impact stiffness employed in analysing bridge pounding [27]. In building pounding analysis, the impact stiffness used is assumed to be equivalent to the axial stiffness of the building's slab. [25]. Cole et al. [47] derived a novel equation to determine an impact stiffness value by considering both the characteristics of the colliding elements and the time duration of the impact. Xu et al. [48] created a different equation for the impact stiffness of a linear model and contrasted it with the axial stiffness method and the Cole formula. The findings indicated that the new equation yielded more precise outcomes than the two studied formulas.

The structural response assigned to the pounding did not account for a high value for an impact stiffness coefficient. Thus, Ghandil & Aldaikh [49] initiate that the pounding reaction is indifferent to the coefficient of impact stiffness when its value exceeds 1010 N/m. On the other hand, Naserkhaki et al. [50] proposed that the coefficient of impact stiffness supposed to be 50 to 100 times higher than the building’s lateral stiffness. Defining the appropriate  $k$  value is vital to making certain that the results are valid. An unsuitable value of  $k$  may have direct effects on the peak force and number of impacts between the adjacent buildings. At present, there is no relationship developed to bridge the gap in terms of impact modelling.

The purpose of the present article is to develop a formula for the impact stiffness  $k$  for the linear viscoelastic model on the basis of the experimental data. This study involved conducting shaking table experiments to simulate floor-to-floor pounding between multistorey buildings at different elevations, and the outcomes are presented. The accuracy and effectiveness of the derived experimental value are evaluated and verified by comparing it with the results of theoretical analysis. Figure 1 shows a flowchart for the methodology implemented in this research. The flowchart explains the steps involved in calculating the impact stiffness  $k$ , coefficient of restitution  $e$ , and impact damping  $\xi$  derived from four different earthquake models and using various gaps between adjacent structures.

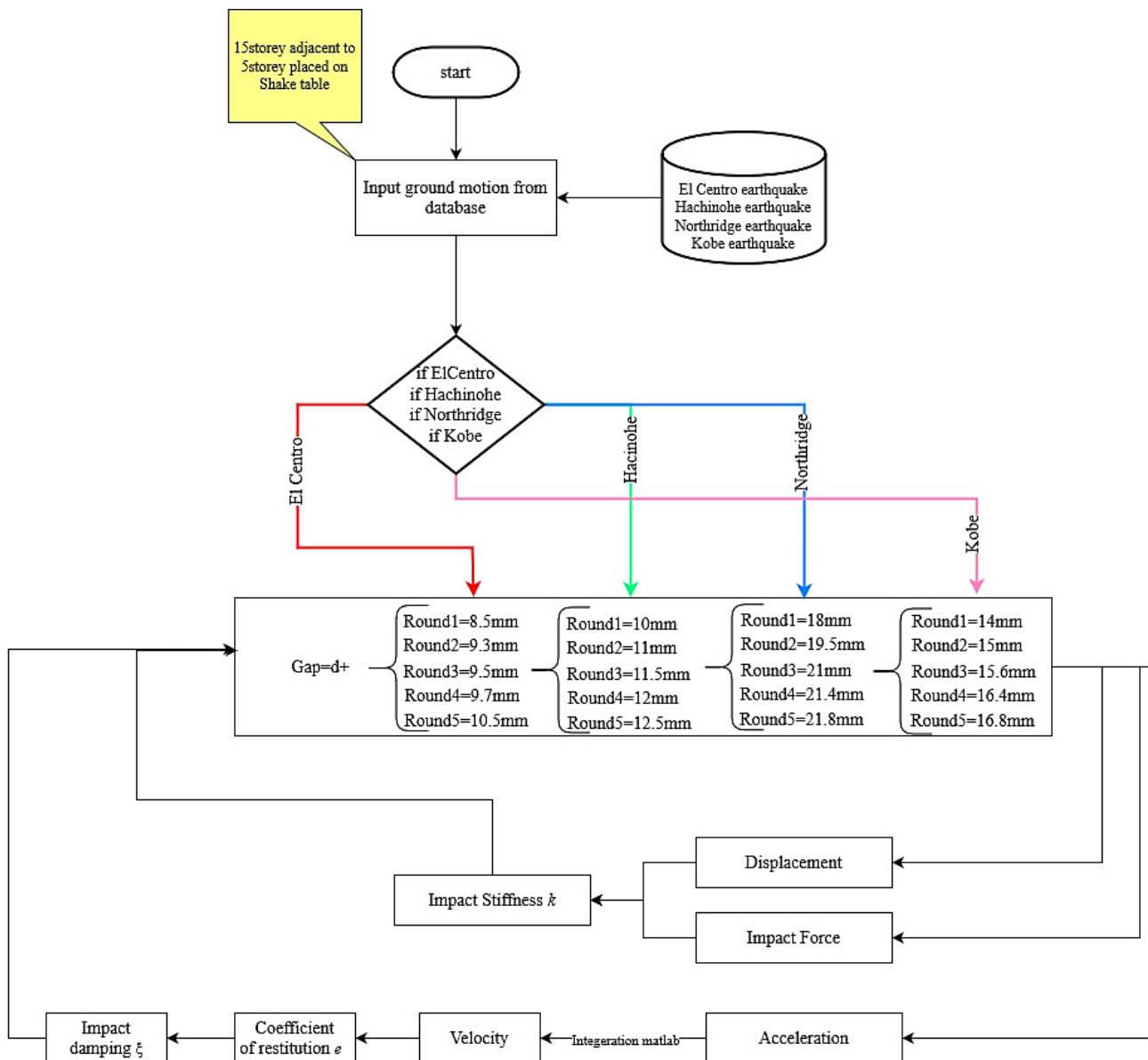


Figure 1. Flowchart for the implemented methodology

## 2. Linear Viscoelastic Impact Model

The linear viscoelastic model, which is also known as the Kelvin–Voigt model, is a widely used method to simulate seismic pounding. This model incorporates a linear spring that models the impact in conjunction with a damper that estimates the amount of energy dissipated during the collision, as shown in Figure 2.

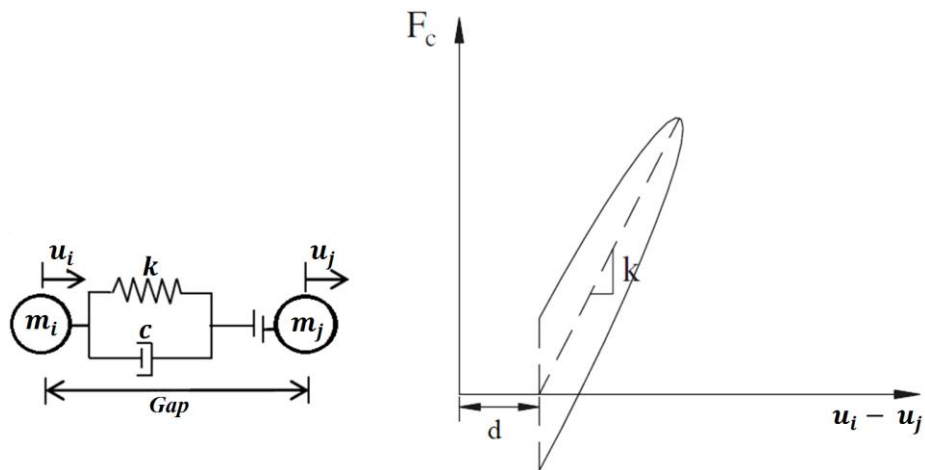


Figure 2. Linear viscoelastic model and contact force-deformation relation

This model has been utilised by several researchers [28, 29, 51, 52]. The impact force,  $F_c$ , in accordance with the model is defined in equations 1 to 4.

$$F_c = \begin{cases} k(u_i - u_j - d) + C(\dot{u}_i - \dot{u}_j); & u_i - u_j - d \geq 0 \\ 0; & u_i - u_j - d < 0 \end{cases} \quad (1)$$

$$C = 2\xi \sqrt{k \frac{m_i m_j}{m_i + m_j}} \quad (2)$$

$$\xi = -\frac{\ln e}{\sqrt{\pi^2 + (\ln e)^2}} \quad (3)$$

$$e = \frac{v_j - v_i}{v_{0i} - v_{0j}} \quad (4)$$

where  $(u_i - u_j)$  and  $(\dot{u}_i - \dot{u}_j)$  are the relative displacements and velocities among the colliding elements at time  $t$ , respectively.  $d$  is the separating gap between the colliding elements. The damping coefficient is  $C$  and  $\xi$  known as the damping ratio. These can be linked to the coefficient of restitution by associating the energy losses throughout the impact. In addition,  $m_i$  and  $m_j$  are the masses of the colliding elements while  $v_{0i}$ ,  $v_{0j}$  and  $v_j$ ,  $v_i$  are the velocities of the crashing masses before impact and after impact, respectively. One drawback of the linear viscoelastic model is that it generates negative pounding forces caused by damping before the colliding structures separate. This results in comparable dissipation throughout both the approach along with restitution stages, which is not in line with actual behaviour [22, 34]. Despite this limitation, much commercial software frequently uses the linear viscoelastic model for simulating structural pounding.

### 3. Related Work in Impact Stiffness

Various methods are employed to determine the impact stiffness. The spring component  $k$  is employed to evaluate the stiffness of the buildings by the contact point, which corresponds to the axial stiffness of the stronger structure [53].

1. Maison & Kasai [43] suggested a straightforward and fundamental formula for the impact stiffness coefficient  $k$ , illustrated in Equation 5.

$$k = \frac{EA}{L} \quad (5)$$

where  $E$  is the elasticity modulus and  $A$  and  $L$  are the area and the length of the crashing structural elements of the building, respectively.

2. Naserkhaki et al. [50] proposed a succeeding equation proceeds on the assumption that the building's lateral stiffness should be multiplied by a coefficient of 50 to 100 to obtain the appropriate impact stiffness.

$$k = \text{Building stiffness} \times (50 - 100) \quad (6)$$

3. Based on the experiment performed by Jankowski [44], the impact stiffness parameter value for steel-to-steel impact was  $k = 482 \text{ kN/mm}$  under the linear viscoelastic model.
4. Xu et al. [48] developed the following formula for an impact stiffness (Equation 7) of the linear viscoelastic model:

$$k = \frac{m_j}{m_i + m_j} k_1 e^{(2 \ln e / \pi) \left( \arcsin \left( \pi / \sqrt{\pi^2 + (\ln e)^2} \right) \right)} \quad (7)$$

where  $k_1$  is calculated based on Equation 5.

## 4. Testing Program

### 4.1. Experimental Method

An experimental study has been designed on the basis of the shaking table concept. The aim of the experiment is to exhibit the impact stiffness  $k$  of the linear viscoelastic model for seismic pounding. The experiment should consider the different heights of adjacent buildings. The two model buildings were placed on the shaking table with a view to simulating earthquakes with a certain gap between the buildings. The gap was carefully chosen to allow pounding between the adjacent buildings in order to study seismic response, including acceleration, displacement, and impact force. The experimental data were taken from three different sensors placed on the adjacent buildings. The sensors collected three variables, namely, acceleration, displacement, and impact force time histories. The three variables were analysed using MatLab to obtain the velocity from the acceleration data. The stiffness concerning the contact element  $k$  was established by plotting the experimental impact force-displacement correlation.

### 4.2. Earthquake Simulator

The experimental work was carried out on the multi-axial simulation table type MTS 354.20 at the structural testing facility in the state-of-the-art Tech Lab at the University of Technology, Sydney. The shaking table has plane dimensions of 2.2 m  $\times$  2.2 m with six degrees of freedom. The shaking table used in the study has a capacity of testing samples up to 2 tonnes and can provide acceleration up to 5 g, velocity up to 1000 mm/s, and stroke up to  $\pm 200$  mm. The system can be used as an earthquake simulator and is powered by six hydraulic actuators in a hexapod arrangement with a highly sophisticated control system to ensure the waveform is accurately reproduced.

### 4.3. Tested Frames

The experimental program examined steel-frame models of 15-storey and five-storey buildings in 1/30 scale. According to AS/NZS 3678-2011, the two frame constructions were each individually developed at their smaller scale (in structural steel). The tested frames were created using a methodology used by Tabatabaiefar et al. [54]. All versions have a floor plan that measures 0.4 m by 0.4 m overall. The 15-storey frame is 1.5 m tall, while the five-storey frame is only 0.5 m tall. Columns along with floors in the models were constructed from sections of flat steel with a rectangular shape measuring 40 mm by 2 mm and 400 mm by 5 mm, respectively.

### 4.4. System Identification of the Steel-Frame Models

Through the execution of many initial tests, including free vibration, frame stiffness and a sine sweep test, the dynamic properties of individually steel frame were established. The experiment's goal in the free vibration testing was to determine the structures' fundamental period and damping. There are numerous ways to calculate damping. One technique is to use the structure's frequency response function's width of peak value [55, 56]. The stiffness test was created to gauge the frame structure's stiffness parameter. The sine sweep test was conducted to determine the natural frequency and vibration modes, specifically modes one, two and three. The dynamic properties of the experimental along with the numerical findings for the 15-storey and five-storey steel models are shown in Table 1.

**Table 1. Structural model's dynamic characteristics assessed through experiments and numerical analysis**

	Experiment					Numerical				
	Free Vibration		Sine Sweep Test			Stiffness kN/mm	Modal Load Analysis			Stiffness kN/mm
	Natural Frequency Hz	Damping %	Mode 1 Hz	Mode 2 Hz	Mode 3 Hz		Mode 1 Hz	Mode 2 Hz	Mode 3 Hz	
<b>5-storey</b>	6.53	0.467	6.43	19.99	35.91	0.0275	6.42	19.275	31.544	0.0278
<b>15-storey</b>	2.27	0.503	2.113	6.695	11.57	0.0083	2.0976	6.285	10.455	0.0087

### 4.5. Selected Seismic Acceleration Records

The four scaled earthquake ground motions utilised in the shaking table experiments are El Centro 1940 (Figure 3-b), Hachinohe 1968 (Figure 4-b), Northridge 1994 (Figure 5-b) and Kobe 1995 (Figure 6-b) [57]. The first two quakes were characterised as distant ground motions (far-field), whereas the last two were considered nearby earthquakes (near-field). Near-field earthquakes have a distinct impact on structures compared to far-field earthquakes. When developing buildings, the discrepancy between the two circumstances must be taken into consideration [58]. The properties of near-field ground motion have received significant attention from researchers in determining elastic along with inelastic behavioural dynamic of a structure [59, 60]. The International Association for Structural Control and Monitoring selected these four earthquakes as a standard for seismic investigations [61]. The recordings contain multiple excitation frequency mixtures, varied acceleration amplitudes and different time scales. These seismic records also differ in terms

of distance to the epicentre. Regarding the peak ground acceleration (PGA), the Northridge earthquake had the greatest value out of the four seismic events considered. The earthquake's PGA is 0.843 g, and its epicentre is lower than 9.2 km away. The Kobe earthquake occurred at a distance of 7.4 km and had a peak ground acceleration of 0.833 g. The El Centro earthquake had a PGA of 0.349 g (calculated at a distance of 15.7 km). Finally, the Hachinohe earthquake's PGA was 0.229 g, and its epicentre was less than 14.1 km away.

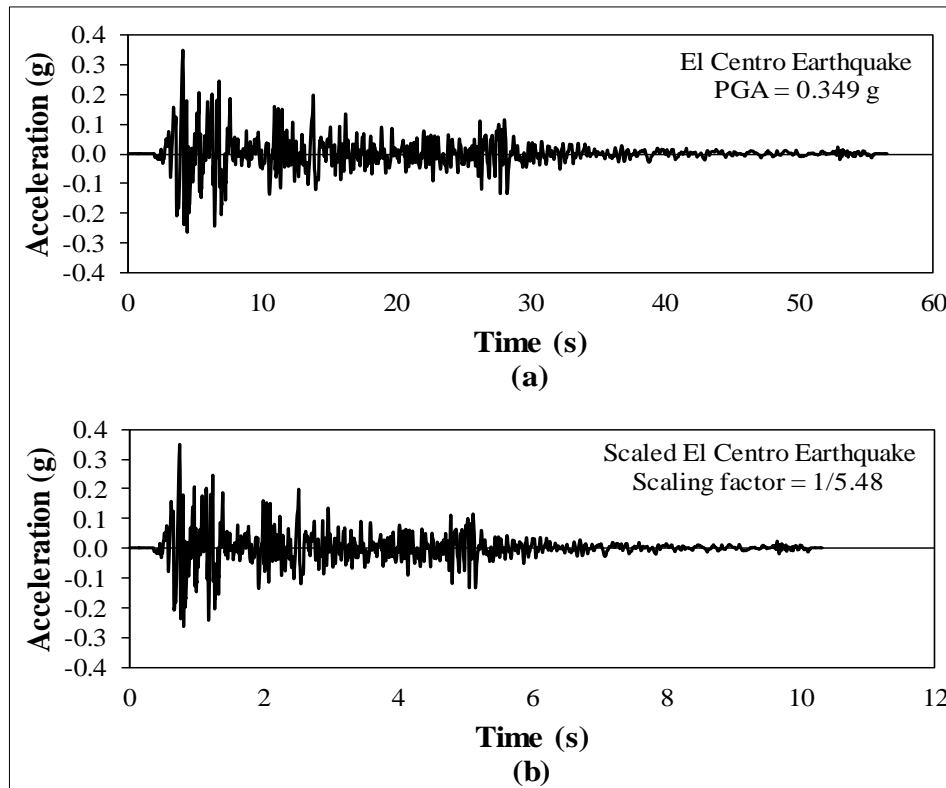


Figure 3. El Centro earthquake 1940, with (a) representing the primary record and (b) representing the resized record

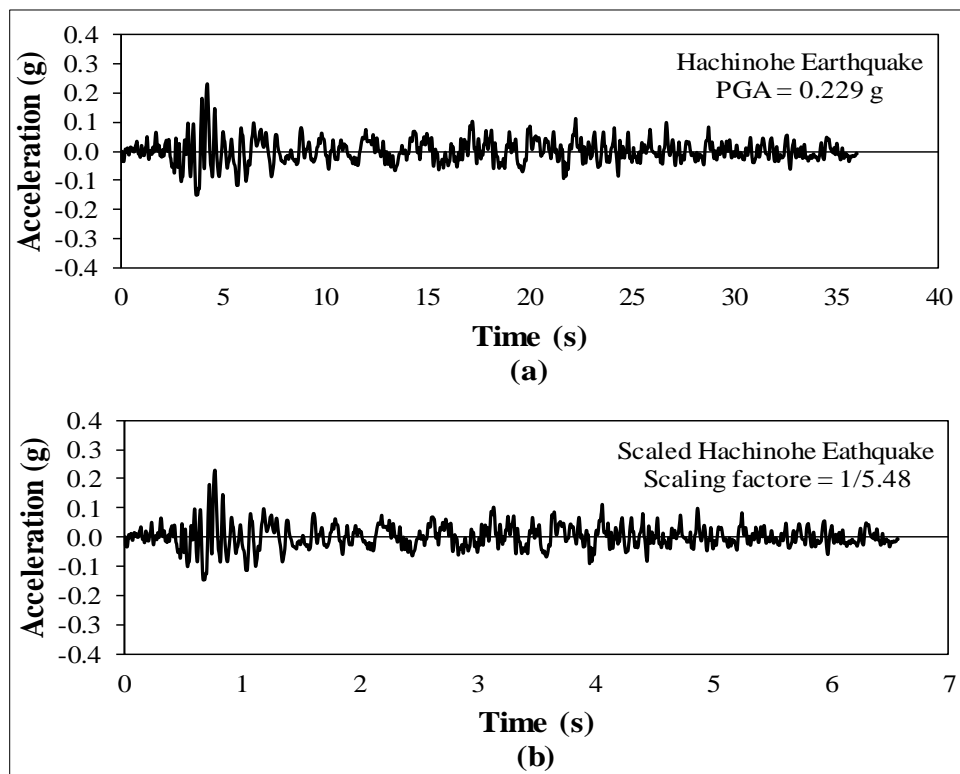


Figure 4. Hachinohe earthquake 1968, with (a) representing the primary record and (b) representing the resized record

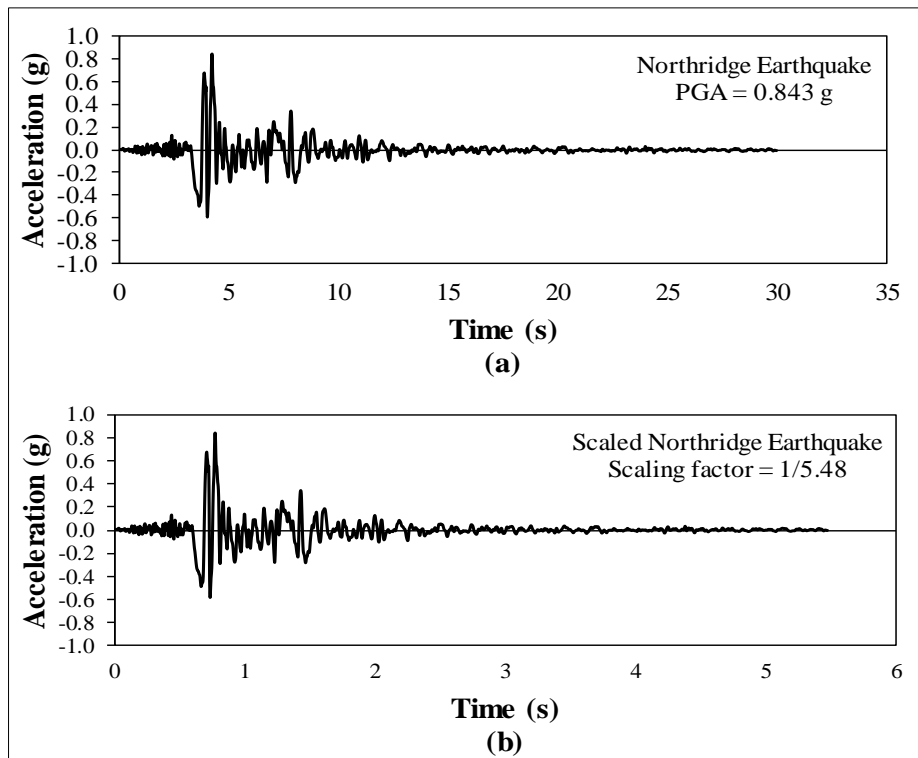


Figure 5. Northridge earthquake 1994, with (a) representing the primary record and (b) representing the resized record

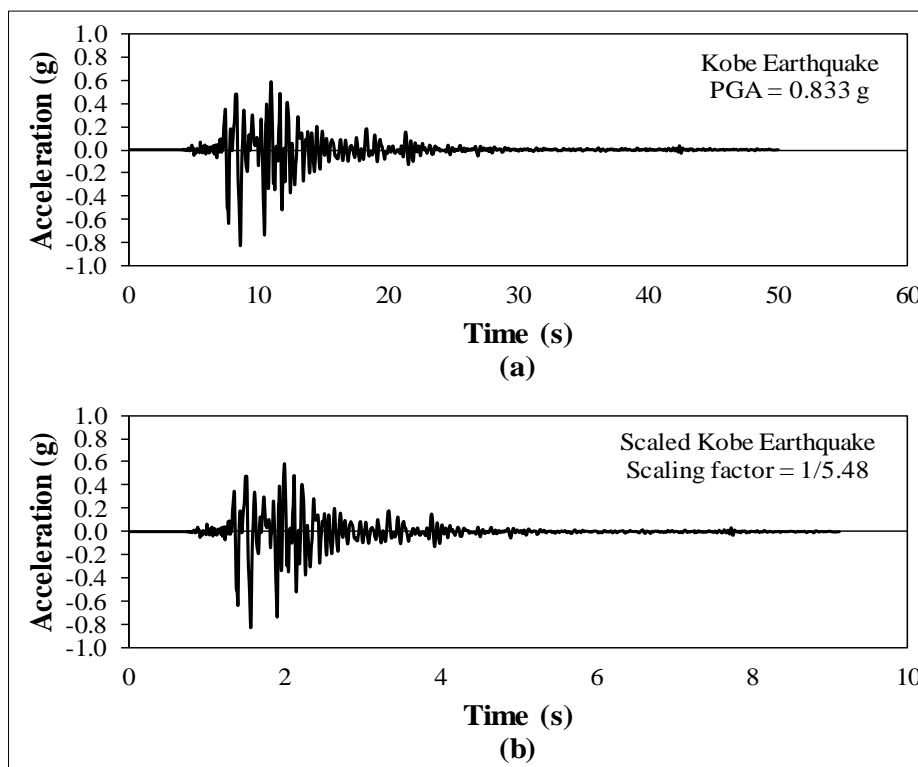


Figure 6. Kobe earthquake 1995, with (a) representing the primary record and (b) representing the resized record

#### 4.6. Test Set-Up

The frame models used in the experiment were positioned and fixed onto the shaking table to represent a 15-storey structure adjacent to a five-storey structure. As shown in Figure 7-a, once the experimental models were secured to the shaking table, the accelerometer sensors and laser sensors for displacement (LD) were mounted. A force sensor was also placed at the point of impact. The sensors were utilised to measure the pounding force, acceleration along with displacement response of the impact. Shaking table tests were conducted using scaled earthquake acceleration recordings (Figures 3 to 6). The reference frames are located outside of the shaking table. Therefore, the displacements that have been recorded are the absolute displacement time history.

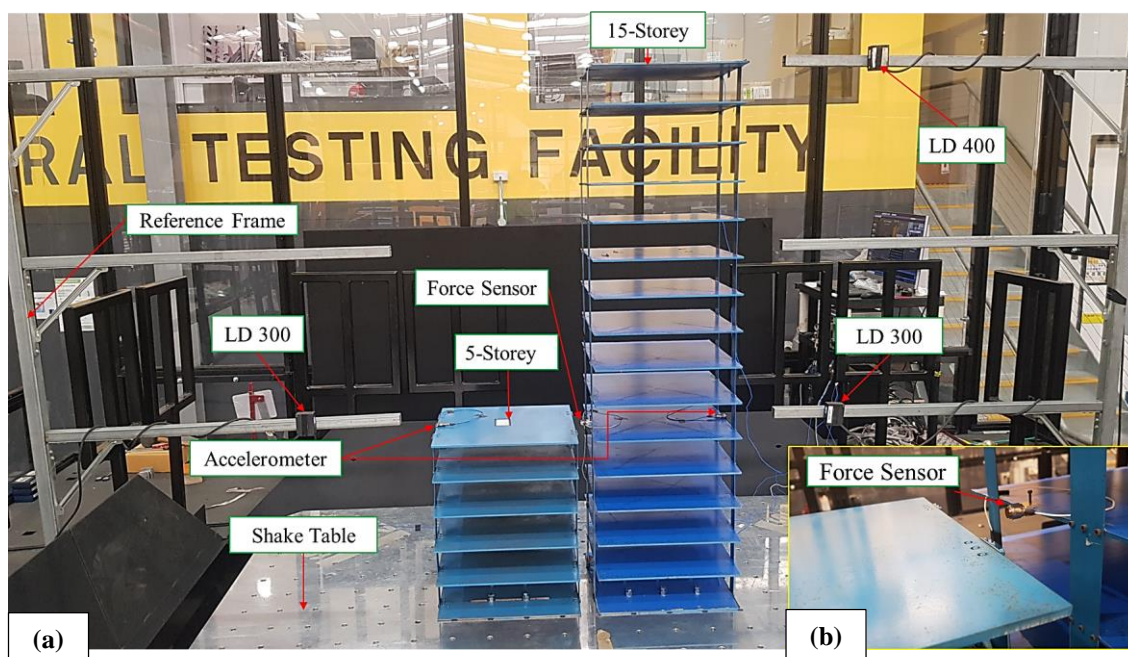


Figure 7. Test frames on shake table

Using scaled El Centro earthquakes, the coupled steel frames were evaluated with separation gaps of 10.5 mm, 9.7 mm, 9.5 mm, 9.3 mm and 8.5 mm. Under the scaled Hachinohe earthquake, the separating gaps were 12.5 mm, 12 mm, 11.5 mm, 11 mm and 10 mm. The neighbouring steel frames were evaluated with separating gaps of 21.8 mm, 21.4 mm, 21 mm, 19.5 mm and 18 mm under the scaled Northridge earthquake, and the separation gaps under the scaled Kobe earthquake were 16.8 mm, 16.4 mm, 15.6 mm, 15 mm and 14 mm. Separating distances were established based on a previous experiment we carried out to ascertain the lowest safe space to avoid pounding. The spacing between the components was meticulously designed to ensure the elasticity of the system remains intact and to detect pounding without compromising the stability of the structure. It is important to mention that none of the conducted tests showed any appreciable torsional motion [62].

The sensors were arranged as follows: accelerometers of type PCB 352C34 ( $\pm 50$  g) were mounted on the fifth and 15th floors of the 15-storey frame and the fifth floor of the five-storey frame, respectively. Two LD300 laser sensors for displacement (with a range of  $\pm 150$  mm) were mounted on the reference frames, one opposite the fifth floor of each frame, and one LD400 sensor (with a range of  $\pm 200$  mm) was mounted opposite the 15th floor of the 15-storey frame. A force-measuring device was secured to the fifth floor of the pliable left frame, positioned directly across from the steel plate of the inflexible right frame that would bear the impact force. A more extensive perspective of the intersection point between the two frames is presented in Figure 7-b. The force generated by the impact due to pounding was measured using a force sensor of type PCB 208C05 (with a range of measurement of 22.24 kN).

## 5. Experimental Results

More than 50 pounding experiments between the nearby structural steel models were conducted and subjected to numerous input ground motions and separating distances. To accurately capture the impact force, displacement along with acceleration, the data was sampled by the researchers at 10,000 samples per second. Using four ground motion records that were adjusted in size, and as a result, scaled down, the experiments were conducted and impact force time histories were recorded and analysed (as shown in Figures 13 to 16).

### 5.1. Experimental Impact Parameters

To ascertain the parameters concerning the impact model, for example in case of an impact stiffness  $k$  and impact damping  $C$ , the following steps were implemented:

1. Figures 8–11 illustrate the graphical representation of the experimental correspondence between impact force and displacement. The area beneath each loop in these diagrams stands for the energy used in a collision. The stiffness concerning the contact element is represented by the slope of the figure in any of the loops. According to the experimental findings, the average of stiffness in contact element has been taken as  $k$ -experiment = 20,660 N/mm.



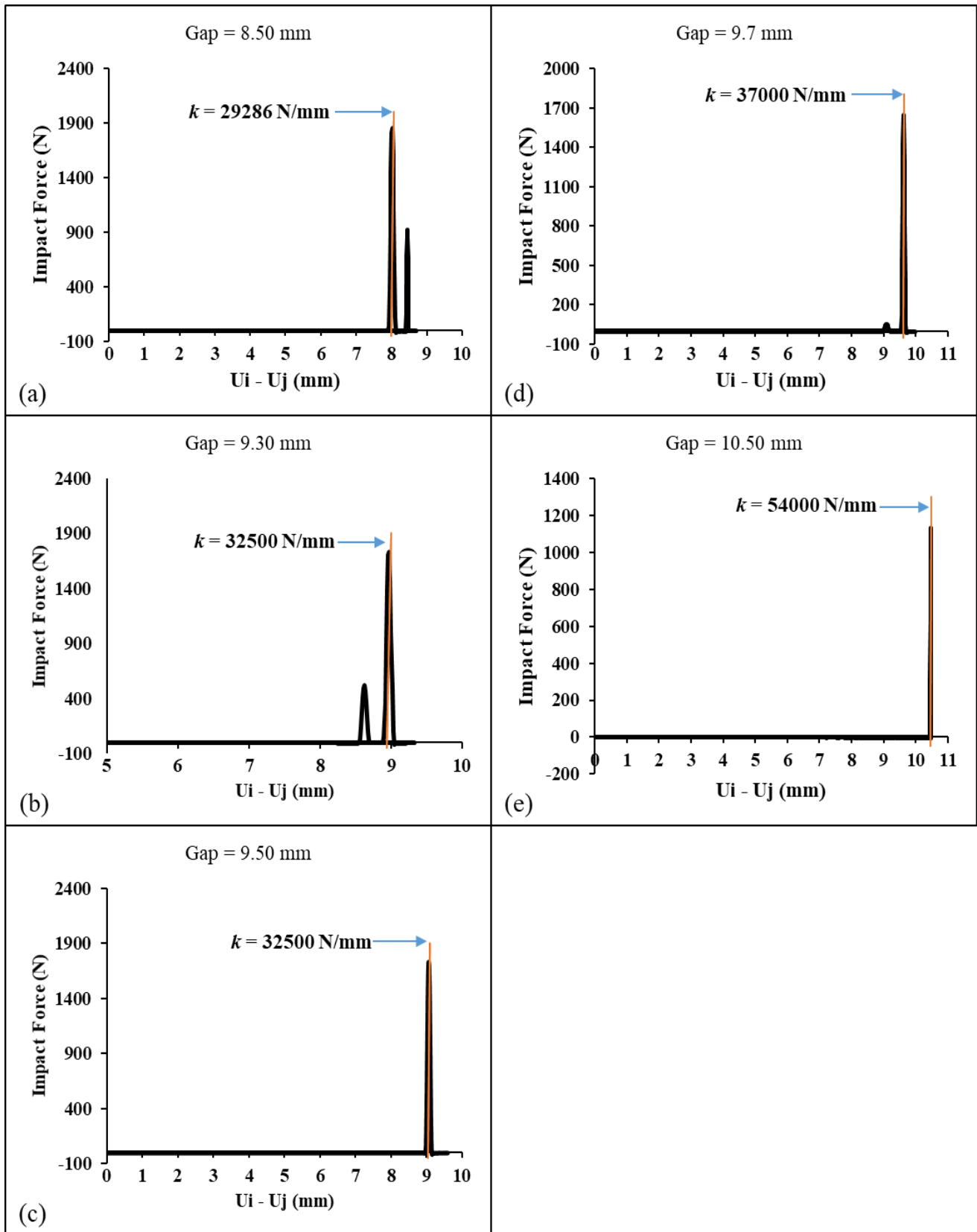


Figure 8. Impact force-displacement relationship for pounding between the coupled 15-storey and five-storey buildings (fifth floor) subjected to scaled El Centro earthquake with gap equal to a) 8.5 mm; b) 9.3 mm; c) 9.5 mm; d) 9.7 mm; e) 10.5 mm

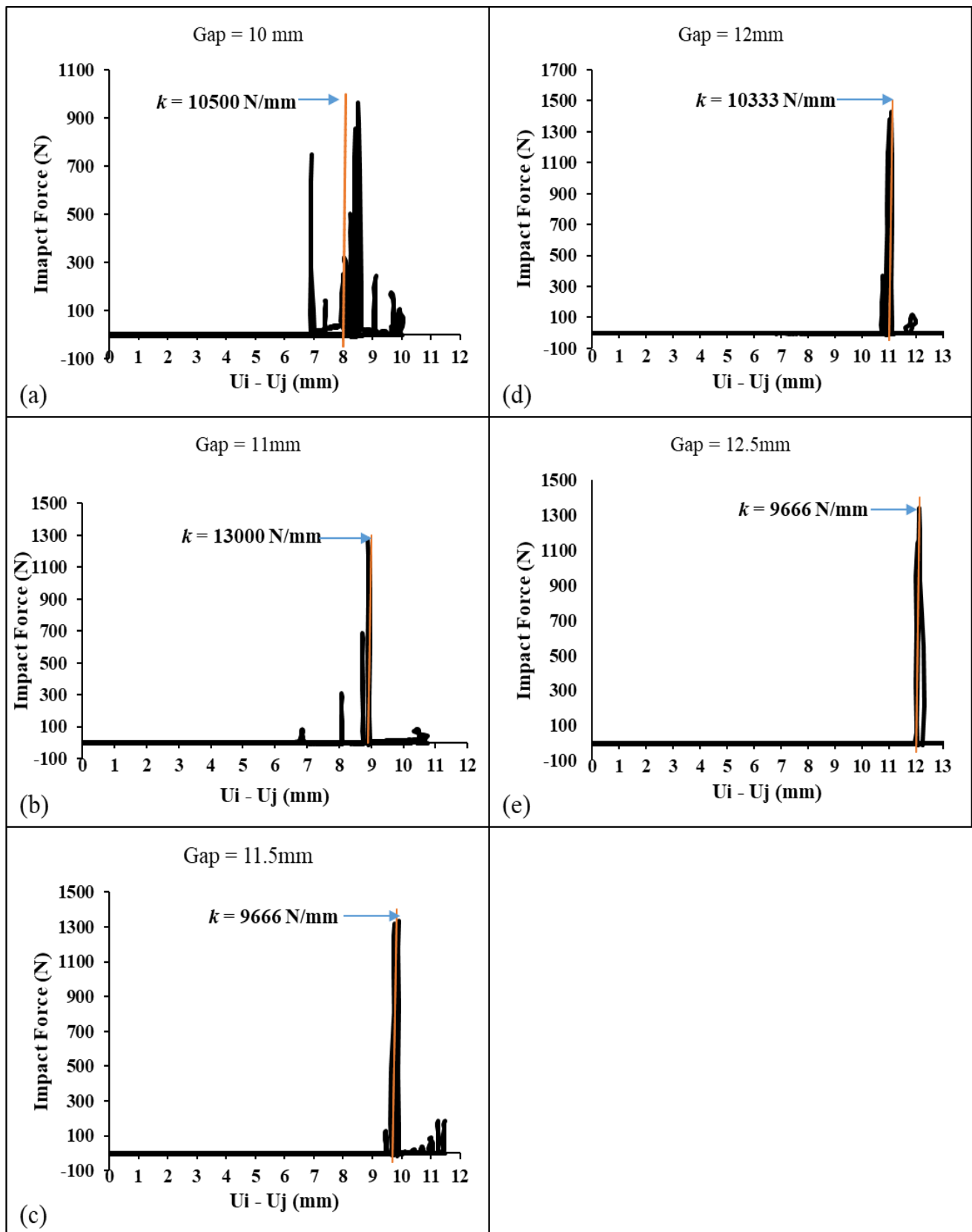


Figure 9. Impact force-displacement relationship for pounding between the coupled 15-storey and five-storey buildings (fifth floor) subjected to scaled Hachinohe earthquake with gap equal to a) 10 mm; b) 11 mm; c) 11.5 mm; d) 12 mm; e) 12.5 mm

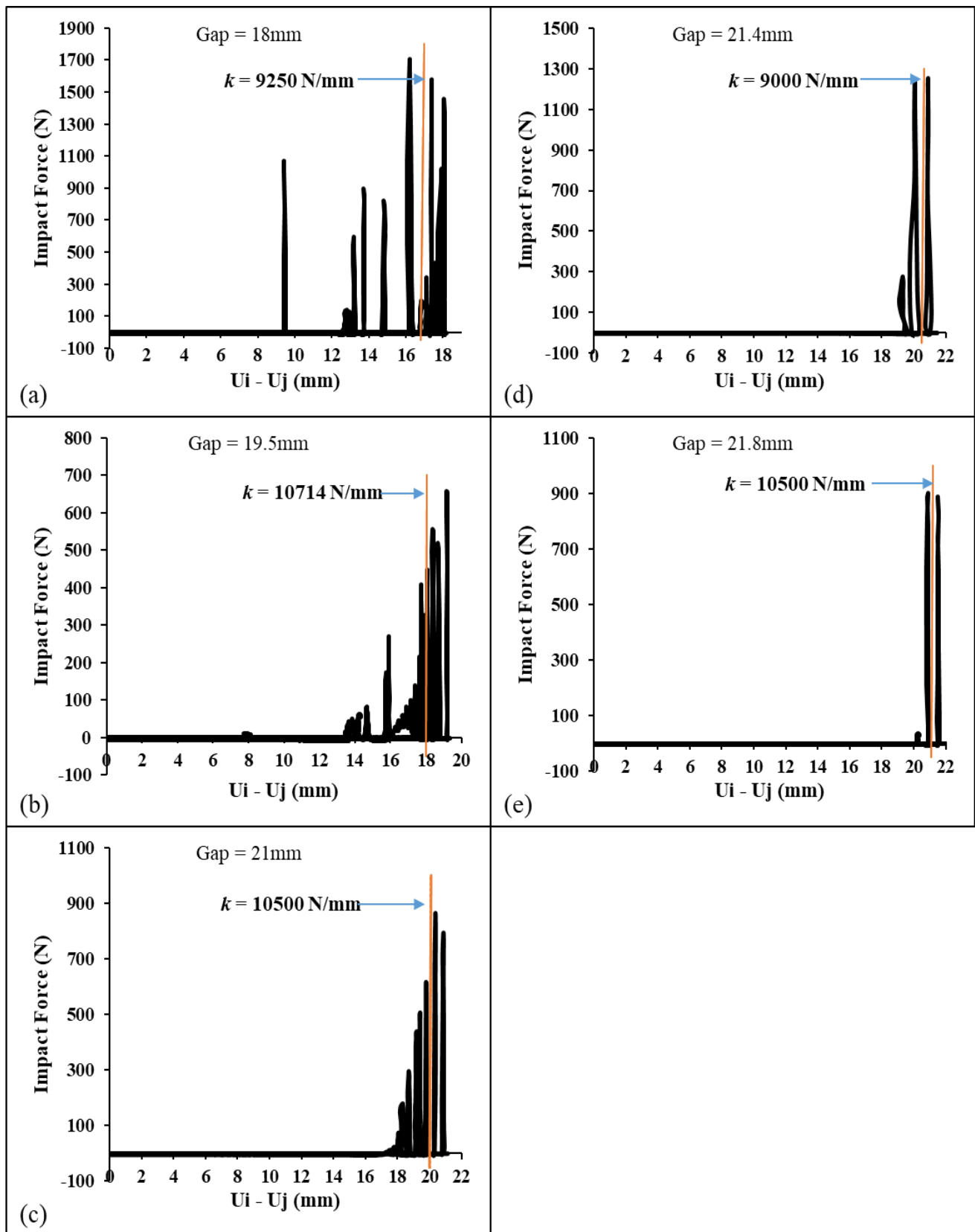


Figure 10. Impact force-displacement relationship for pounding between the coupled 15-storey and five-storey buildings (fifth floor) subjected to scaled Northridge earthquake with gap equal to a) 18 mm; b) 19.5 mm; c) 21 mm; d) 21.4 mm; e) 21.8 mm

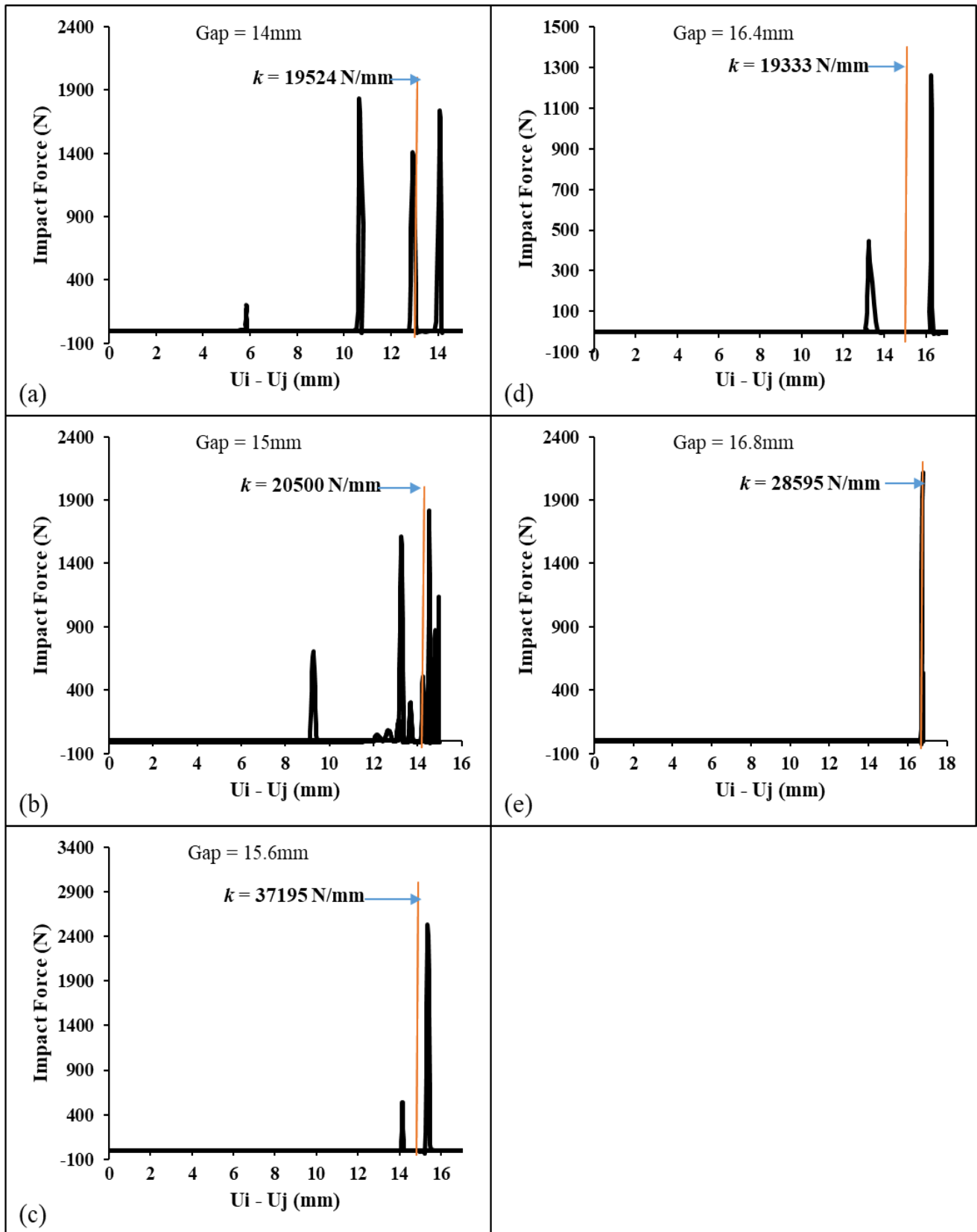


Figure 11. Impact force-displacement relationship for pounding between the coupled 15-storey and five-storey buildings (fifth floor) subjected to scaled Kobe earthquake with gap equal to a) 14 mm; b) 15 mm; c) 15.6 mm; d) 16.4 mm; e) 16.8 mm

2. To derive the velocity time history, the acceleration data recorded at the fifth levels of both the 15-storey and five-storey frames, where the pounding occurred, were subjected to numerical integration using the trapezoidal method. After integration, Pitilakis et al. [63] used a technique that involves applying the high-pass Butterworth filter numerous times to remove drift error and phase distortion. It was decided to implement the aforementioned integration using a MATLAB code.

3. By identifying the velocity at the moment of impact, we were able to compute the numerical values of the velocities pre and post the impact; namely, the velocities of the crashing masses before and after impact  $v_{0i}$ ,  $v_{0j}$  and  $v_i$ ,  $v_j$ , respectively.
4. The coefficient of restitution  $e$  been calculated using Equation (4) based on the velocities pre and post each collision event.
5. Equation 3 was taken into account for calculating the impact damping ratio  $\xi$  at each value of  $e$ . For the full time history record, the average value concerning the coefficient was calculated. Figure 12 illustrates the impact force and the velocity within a short period.

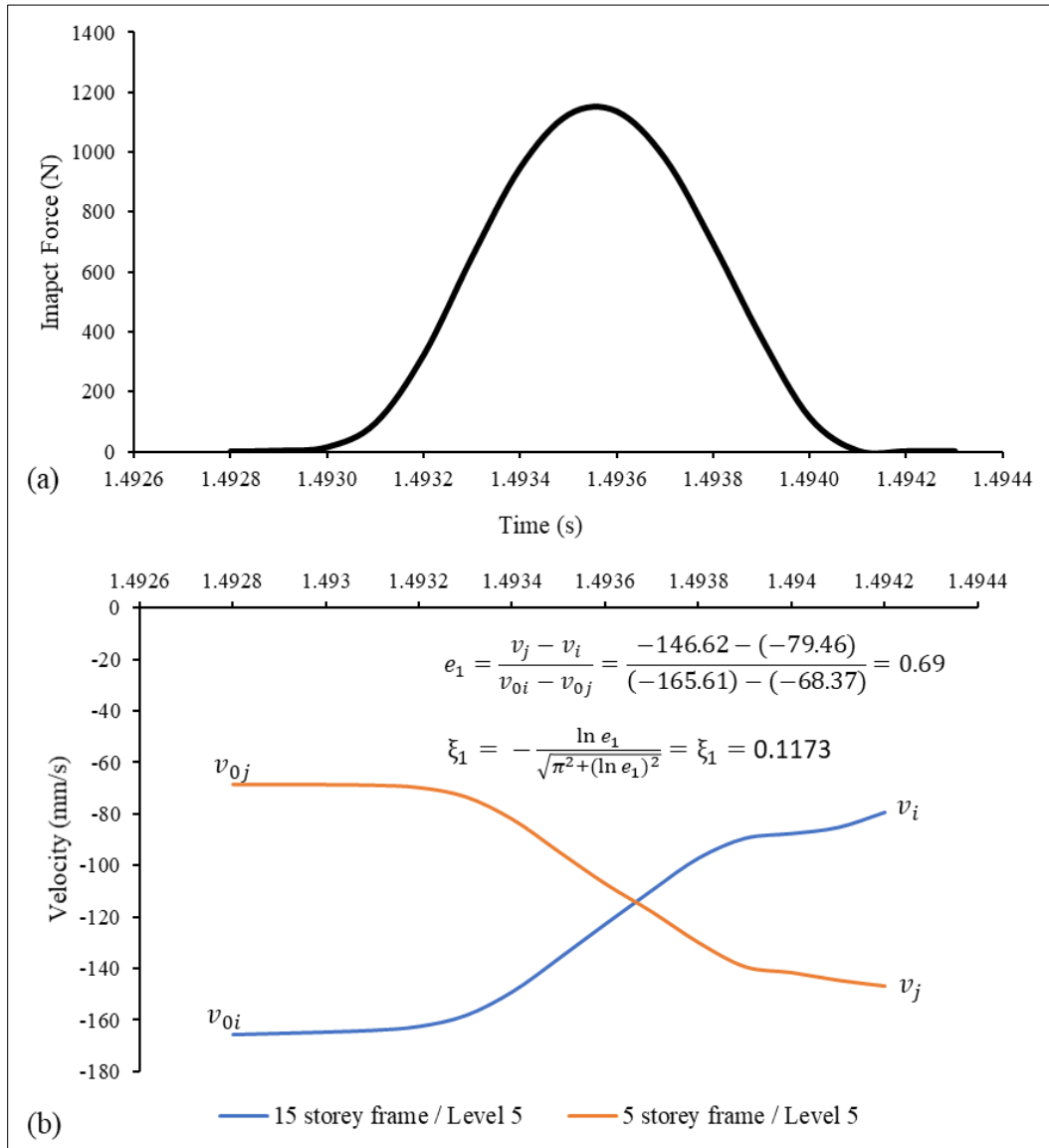


Figure 12. (a) Experimental normal contact impact force within a short time; (b) velocity of 15-storey and five-storey frames at the fifth floor for the same time interval

6. Equation 2 was employed to calculate the dashpot coefficient  $C$  in the contact element.
7. Lastly, the experimental parameters intended for the linear viscoelastic model are  $k$ -experiment = 20,660.0 N/mm,  $C$  experiment = 1255.0 kg/s,  $\xi = 0.078$  and  $e = 0.8$ .

Observations have been made that the range of the restitution coefficient  $e$  utilised to model actual collisions between structures is 0.5 to 0.75 [28]. For typical buildings, Maison and Kasai [43] suggested an interval for  $e$  of 0.53 to 0.85. Guo et al. [41] discovered that the coefficient of restitution for steel bridge structures ranges between 0.86 and 0.96 based on experimental findings. As a result, the computed  $e$  value is considered a suitable value for hammering steel on steel.

## 5.2. Theoretical Formulas for Impact Stiffness

As mentioned earlier, several researchers have carried out studies suggesting numerous assumptions in order to assign a stiffness value  $k$  to the spring element. These values were calculated based on the current experiment as follows:

1. In the experiment, the pounding occurred between the floor slab and the impact cap of the force sensor (called the contact surface). The thickness of the slab steel plate is 5 mm. The impact surface area and length of steel plate are  $A = 63.5 \text{ mm}^2$  and  $L = 400 \text{ mm}$ , respectively. The elasticity modulus is  $E = 2 \times 10^5 \text{ MPa}$  [64]. Equation 5 can be utilised to calculate the impact stiffness parameter as:

$$(k\text{-Masion \& Kasai (1992) [43]}) = \frac{200,000,000 \times 63.5}{400} = 31,750 \text{ N/mm} \quad (8)$$

2. Based on Equation (6) by Naserkhaki et al. [65]

$$(k\text{-Naserkhaki et al. (2013)[65]}) = 0.0275 \times 100 = 2750 \text{ N/mm} \quad (9)$$

3. A 1/30 scale was used in this study. Therefore, according to Jankowski [44],  $(k\text{-Jankowski (2008) [44]}) = 482 \times \frac{1}{30} \cong 16,000 \text{ N/mm}$

4. Developed by Xu et al. [48], according to Equation 7,  $(k\text{-Xu et al. (2016) [48]}) = 12,858 \text{ N/mm}$

Using the aforementioned impact stiffness  $k$ , the researchers calculated the dashpot coefficient  $C$  in the contact element with the help of Equation 2.

Having determined the linear viscoelastic impact model's parameters – namely, the impact stiffness  $k$  along with damping coefficient  $C$  (shown in Table 2) – the impact force time history has been calculated employing Equation 1.

**Table 2. Impact parameters to linear viscoelastic model**

Method	Impact Stiffness $k$ N/mm	Impact Damping Coefficient $C$ kg/s
Experiment	20,660	1255
Masion & Kasai (1992) [43]	31,750	1556
Naserkhaki et al. (2013) [65]	2750	458
Jankowski (2008) [44]	16,000	1104
Xu et al. (2016) [48]	12,848	990

## 6. Discussion

### 6.1. General Comparison

The impact stiffness value ( $k$ -experiment) derived from the experimental measurement was compared to that determined by the other four methods in order to validate the correctness of the derived value. In addition, the accuracy of the current experimental value is validated using theoretical simulations of the pounding response. A comparative study was made based on five methods of determining impact stiffness, to wit: the experimental value ( $k$ -experiment), Masion and Kasai formula (Equation 5), Naserkhaki et al. formula [65] (Equation 6), Jankowski's value and the Xu et al. formula (Equation 7).

To contrast the experimental impact force with the linear viscoelastic model impact force with regard to the impact stiffness obtained from the five methods, Equation 1 was used to calculate the impact force time history. The results are depicted in Figures 13 to 16. The computation was performed using an Excel spreadsheet, and a time step of 0.0001 second was utilised for the analysis. It is evident from the figures that the impact stiffness derived experimentally is evidently different from that determined by other methods. The reason for this discrepancy can be traced back to the sensitivity of the theoretical results and the accuracy with which the dynamic properties of the structures is identified. Correspondingly, impact problems are highly sensitive, and even small changes in the parameters can lead to significant differences in the response.

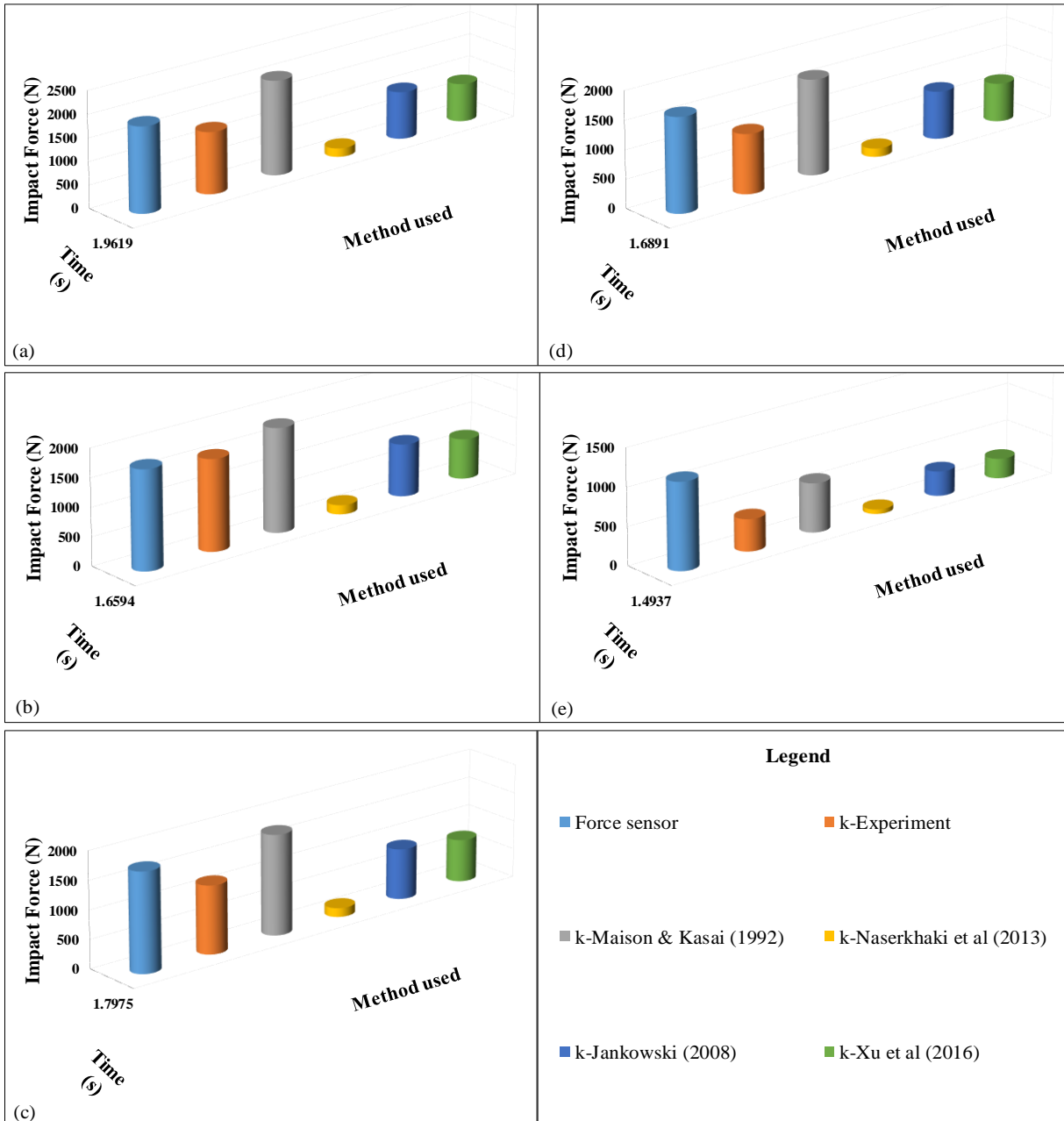
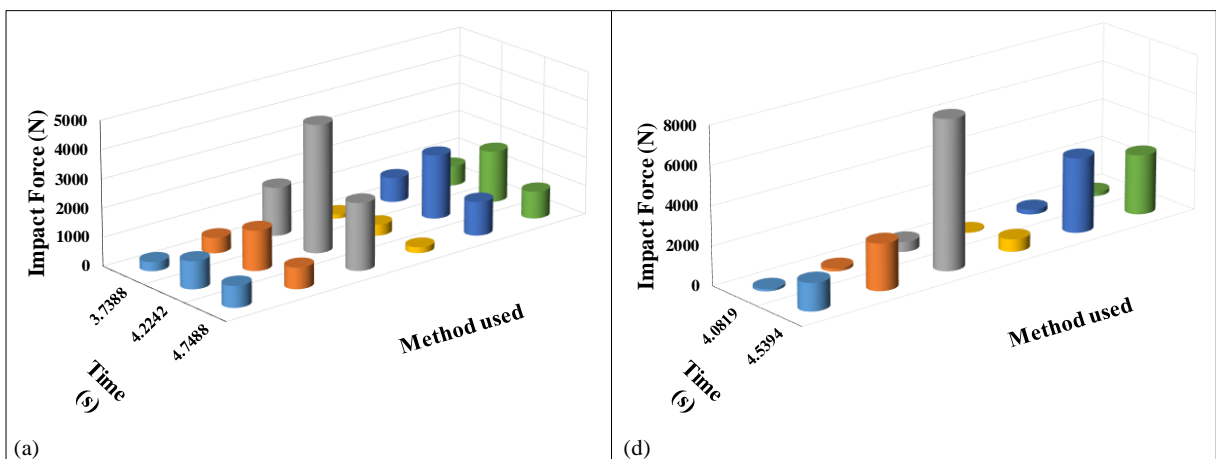


Figure 13. Experimental peak impact force vs theoretical peak impact force with several k values for pounding between the coupled 15-storey and five-storey structures under scaled El Centro with gap equal to a) 8.5 mm; b) 9.3 mm; c) 9.5 mm; d) 9.7 mm; e) 10.5 mm.



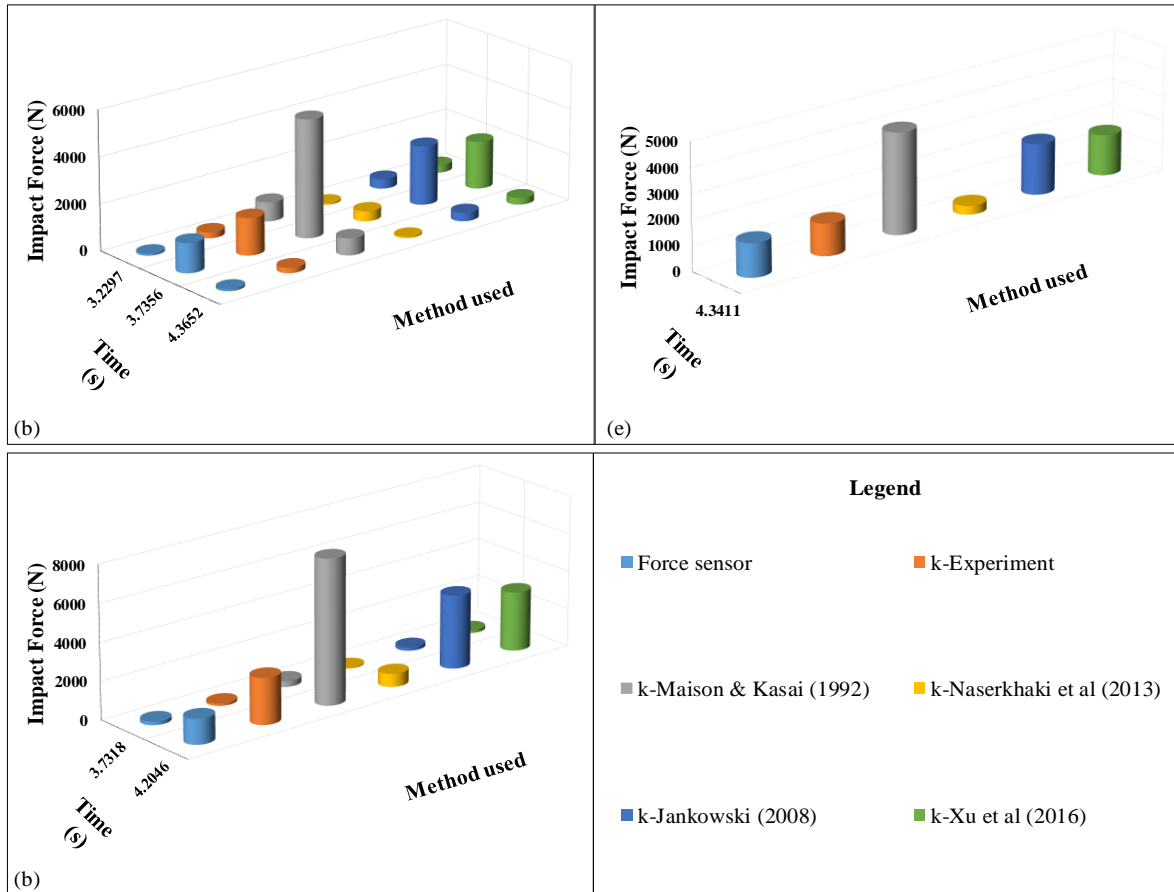
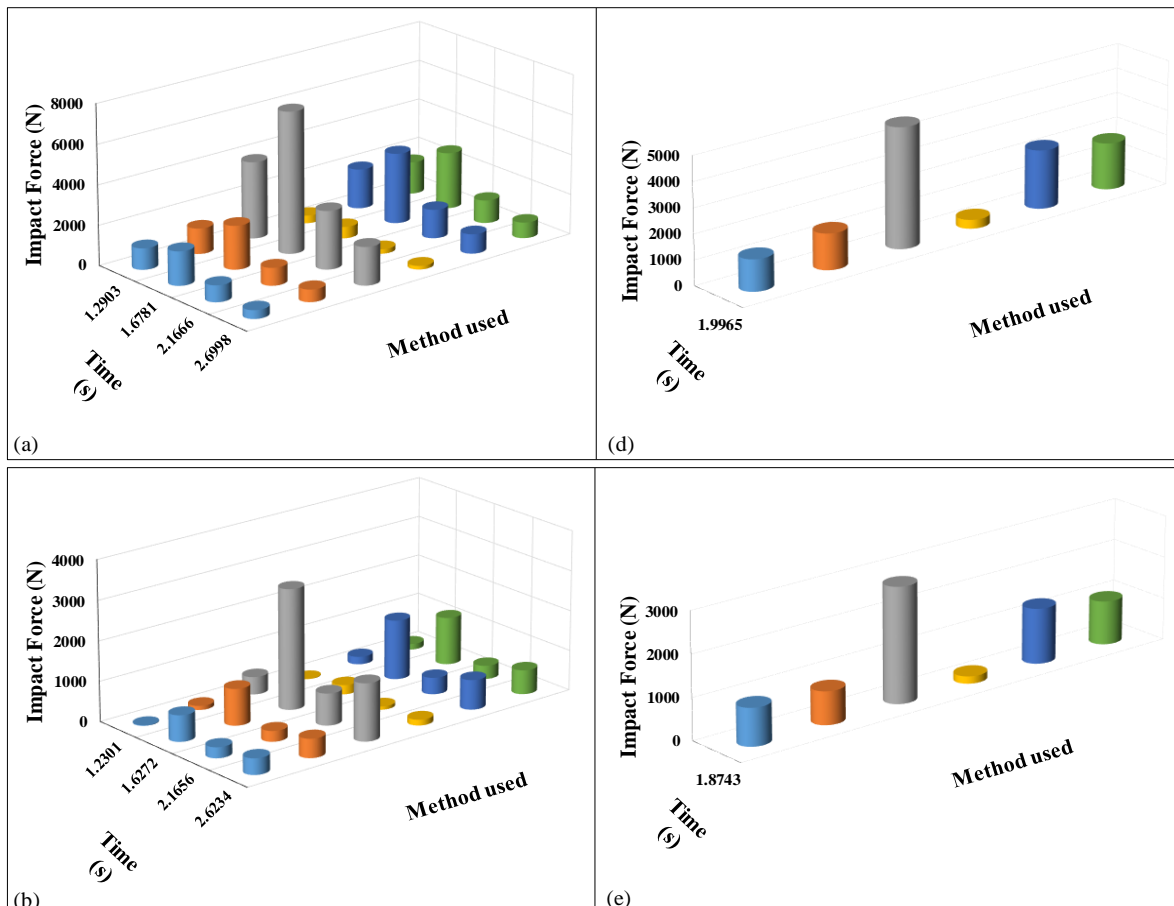


Figure 14. Experimental peak impact force vs theoretical peak impact force with several k values for pounding between the coupled 15-storey and five-storey structures under scaled Hachinohe with gap equal to a) 10 mm; b) 11 mm; c) 11.5 mm; d) 12 mm; e) 12.5 mm.





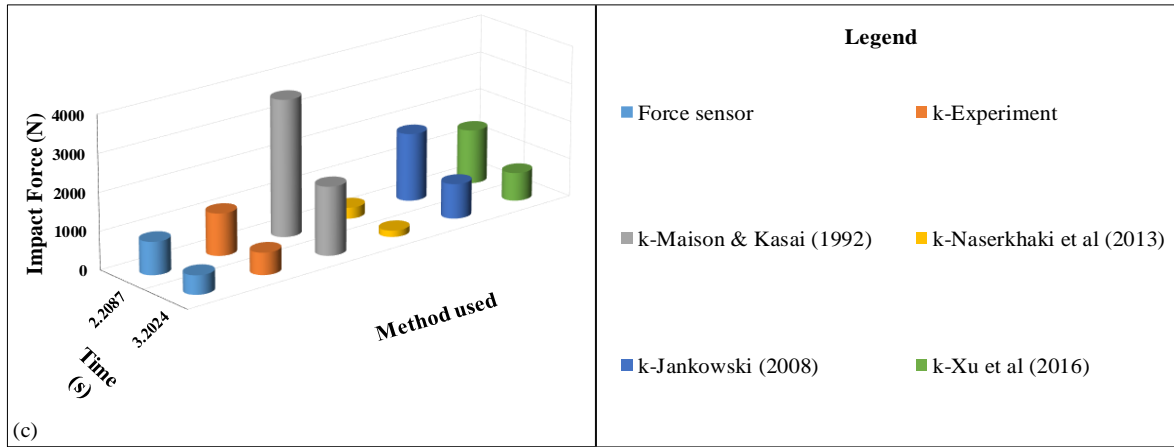


Figure 15. Experimental peak impact force vs theoretical peak impact force with several k values for pounding between the coupled 15-storey and five-storey structures under scaled Northridge with gap equal to a) 18 mm; b) 19.5 mm; c) 21 mm; d) 21.4 mm; e) 21.8 mm

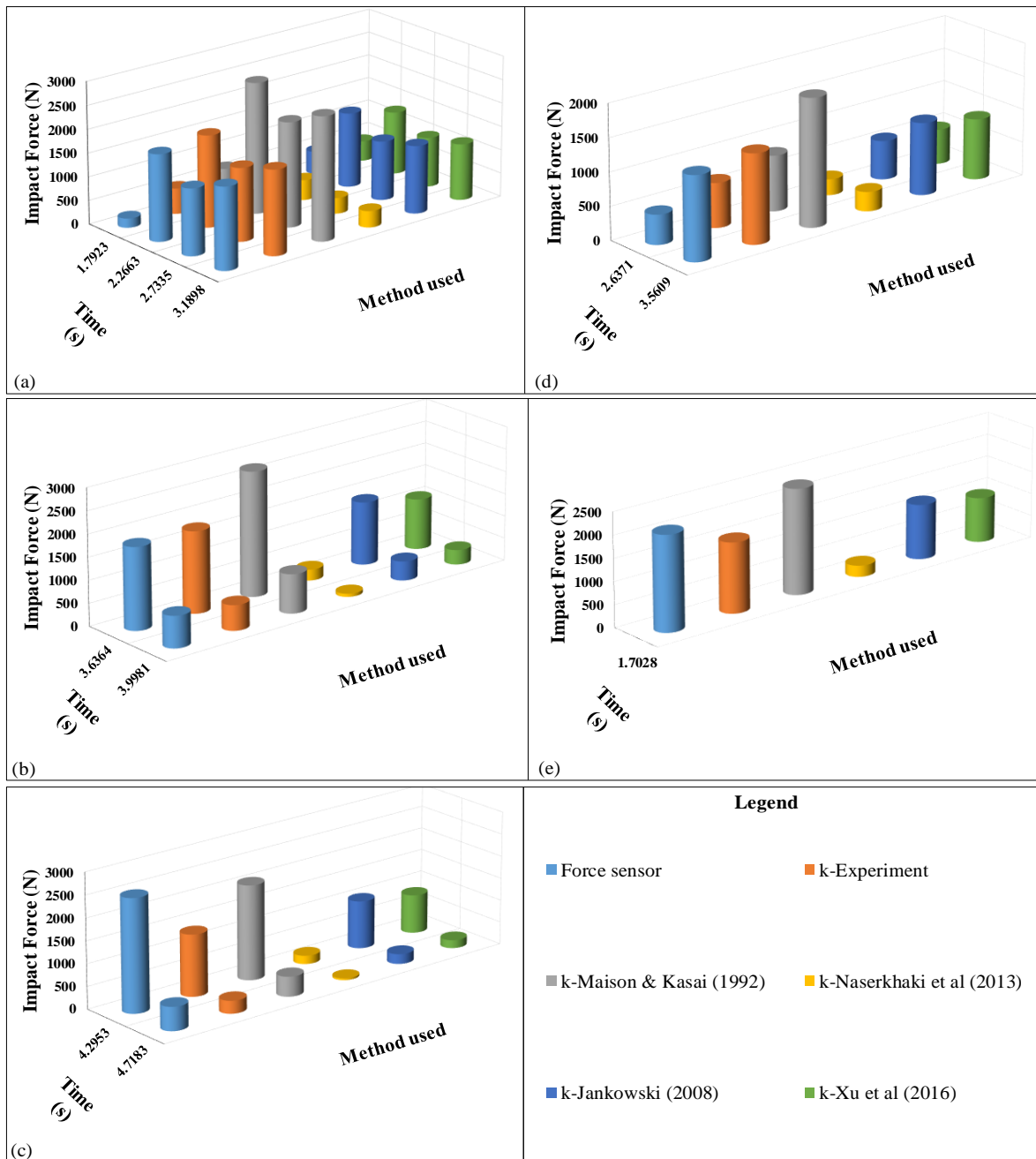


Figure 16. Experimental peak impact force vs theoretical peak impact force with several k values for pounding between the coupled 15-storey and five-storey structures under scaled Kobe with gap equal to a) 14 mm; b) 15 mm; c) 15.6 mm; d) 16.4 mm; e) 16.8 mm

### 6.2. Theoretical Validation

To confirm the accuracy concerning the experimentally determined impact stiffness value, a validation of the peak impact forces obtained from the pounding simulations was performed utilizing the linear viscoelastic model. The impact stiffness obtained using the five methods and similar model factors were utilised in running the theoretical analysis. The difference between the results of the experimental measurement obtained by the force sensor and those of the theoretical analysis was determined through calculating the percent error [66]. The relative error of the peak impact force using the theoretical simulation was obtained using the succeeding formula:

$$E = \frac{|F_{e,max} - F_{t,max}|}{F_{e,max}} \times 100\% \tag{10}$$

where  $E$  is the percent error,  $F_{e,max}$  is the peak impact force on the basis of the experimental measurements and  $F_{t,max}$  is the peak impact force from the theoretical simulation.

Figure 17 displays the discrepancies between the peak impact forces obtained from theoretical simulations utilising the linear viscoelastic model and the impact stiffness calculated from the five different methods, expressed as relative errors. It is apparent from Figure 17 that the experimental value of impact stiffness derived from the linear viscoelastic model had the least relative errors when compared with that of the axial stiffness formula (Equation 5), Naserkhaki et al. formula (Equation 6), Jankowski’s value and the Xu et al. formula (Equation 7). Thus it can be stated that the impact stiffness obtained from the adopted experimental formula of the linear viscoelastic model can produce a more accurate simulation of the structural throbbing than those of other formulas.

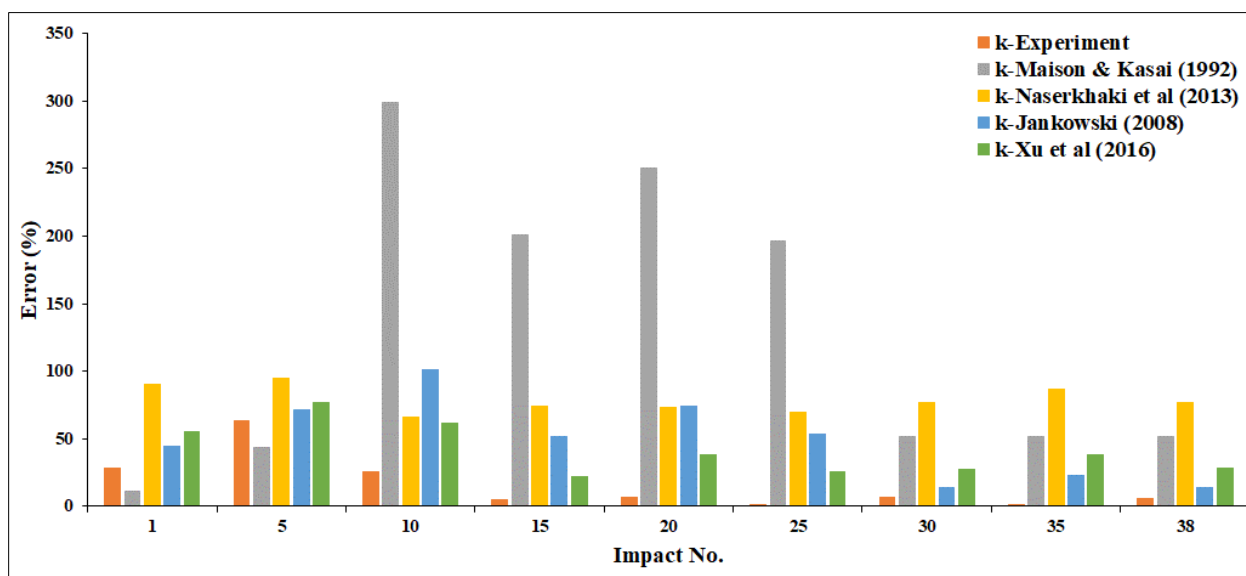


Figure 17. The percent error of the theoretical peak impact forces, based on five types of methods to compute impact stiffness

It should be noted that the outcomes of the current study are valid for elastic response structure only [67]. In this study, it is assumed that the soil beneath the foundations is infinitely inflexible and, consequently, the effects of soil-structure interaction are neglected. The comparison with the theoretical results has confirmed that the adapted formula is sufficiently accurate for practical engineering purposes

The results of this investigation led to the development of the subsequent equation for determining the optimal rescaled impact stiffness  $k$  value:

$$k = 20.66 \times \lambda \times 30 \tag{11}$$

which can be written as

$$k = 620 \times \lambda \tag{12}$$

where  $\lambda$  denotes the scale factor used by the researchers and  $k$  value was measured by kN/mm.

The value of  $k$ -experiment was based on a 1/30 scale factor for single-bay moment resisting steel-framed models. If any other scale factors are employed, then Equation 12 will be used to calculate the new  $k$  value. For instance, if a scale of 1/8 were selected for this model, then the equation result would be:

$$k = 620 \times \frac{1}{8} = 77.50 \text{ kN/mm} \tag{13}$$

### 6.3. Effect of the Mass Ratio and the Coefficient of Restitution

The impact force was examined based on various impact stiffness values, considering different values of parameters, such as the restitution coefficient and the mass ratio of the two crashing bodies. The mass ratio of the two crashing slabs  $m_i$  and  $m_j$  is taken as  $\phi = m_j/m_i$ . The mass ratio  $\phi$  been defined from 0.5 to 5, in increments of 0.2. However, only the impact results due to pounding within the 15-storey building adjoining the five-storey building excited under the scaled El Centro earthquake (far-field) and scaled Kobe earthquake (near-field) were selected for description. It is noticeable in Figures 18 and 19 that the restitution coefficient has a significant influence while mass ratio has no effect on impact force. It was also found that the low value of the restitution coefficient directly affecting the impact force; the negative force is clearly shown in Figure 19. The negative impact force due to pounding simulated by the linear viscoelastic model generated just before separation reported by Jankowski [34, 44] does not have a physical clarification. Nevertheless, choosing the linear viscoelastic model parameters accurately is vital to eliminate the negative impact force, both the impact stiffness  $k$  and the restitution coefficient  $e$  must be set correctly.

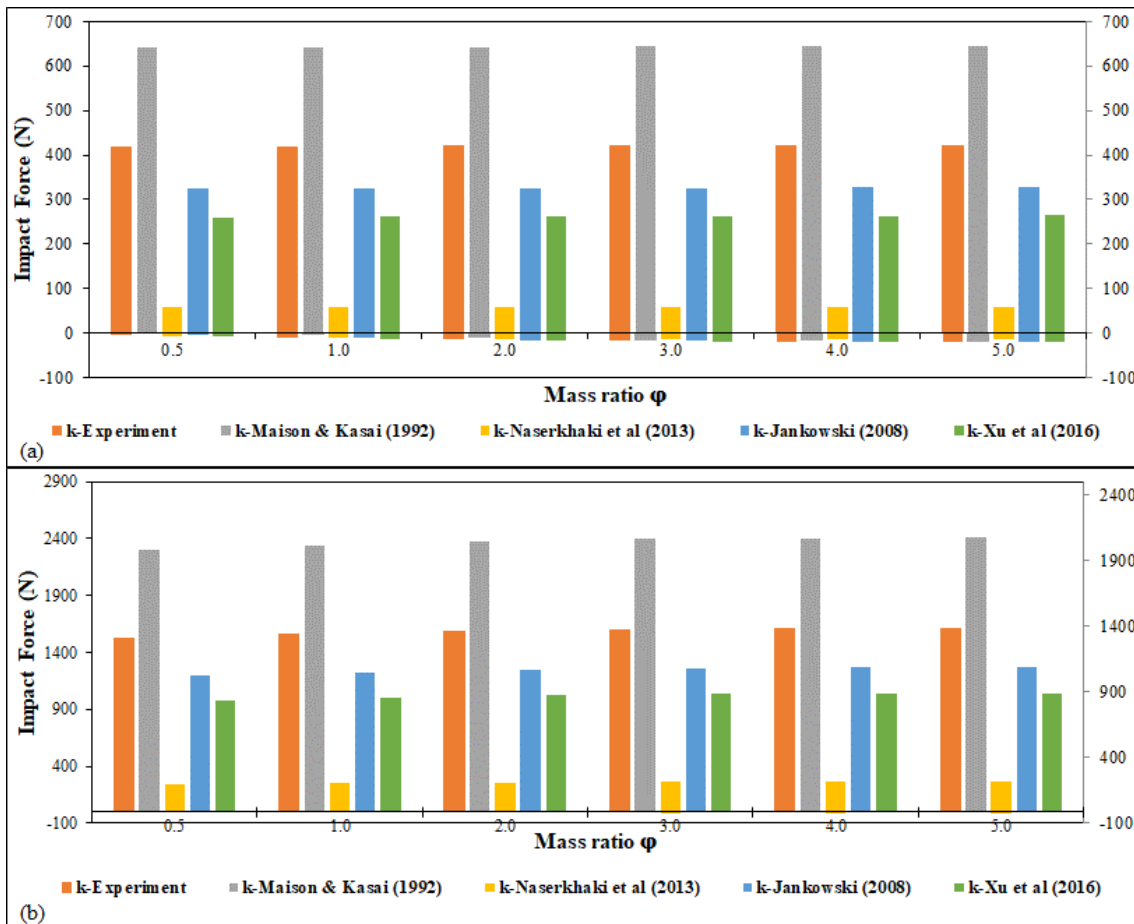
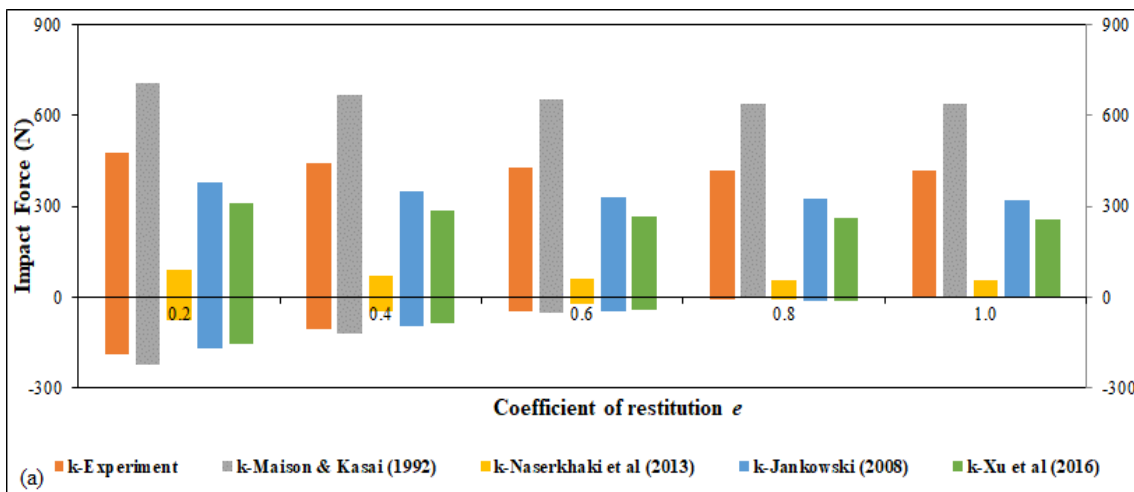


Figure 18. Impact force results obtained from five different methods for varying mass ratios subjected to scaled (a) El Centro earthquake and (b) Kobe earthquake



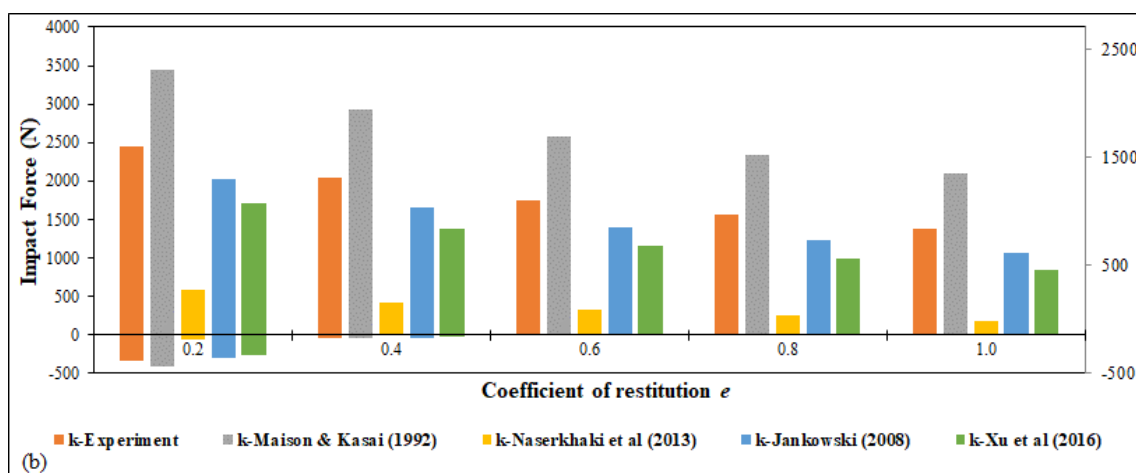


Figure 19. Impact force results obtained from five different methods for varying restitution coefficients subjected to scaled (a) El Centro earthquake and (b) Kobe earthquake

## 7. Conclusion

Experimental tests using an earthquake simulator were conducted on pounding between adjacent steel-frame structures of unequal heights. Two 1/30 scale 15-storey and five-storey steel-frame buildings were considered. The impact forces, acceleration responses and displacement responses due to floor-to-floor pounding were investigated as subjected to various earthquake acceleration records. Based on experimental data from this study, novel equation for calculating the impact stiffness  $k$  of the linear viscoelastic impact model used for simulating pounding was thus developed. The  $k$  values in the experimental data were measured using accelerometers, laser displacement and load cell sensors. The results show the value of the impact stiffness using the linear viscoelastic model compared with the theoretical values advanced by other researchers. Based on the results of our experiments, we conclude that the proposed value of  $k = 620 \text{ kN/mm}$  can be scaled up based on  $k = 620 \times \lambda$ , where  $\lambda$  presents the scale factor. This formula was generated by comparing the theoretical and experimental findings. This theoretical study presented numerical analysis that utilised various earthquakes with different  $k$  values. It was found that the  $k$  value of the experimental study was the most relevant value given the standard deviation and error rate of the numerical analysis.

The simulation of impact force is significantly affected by the impact stiffness along with the coefficient of restitution, whereas the effect of mass ratio of the colliding floors is insignificant.

To validate the accuracy of the suggested  $k$  value, pounding simulation results using the four different formulas were compared. The outcomes of the analysis show that the impact stiffness, derived using the adopted formula of the linear viscoelastic model, is smaller than the axial stiffness concerning the colliding body. The accuracy of the proposed formula was substantiated by comparing the numerical simulation results with the experimental results.

Hence, the present formula concerning impact stiffness considering the linear viscoelastic model is recommended for purposes of obtaining more reliable results when conducting experimental and numerical simulations of earthquake-induced structural pounding.

One suggestion for future research would be to investigate the impact model parameters for various building configurations to gain a better understanding of their impact on simulation accuracy. Moreover, this study focuses on floor-to-floor pounding; further studies are required to conduct column-to-floor pounding as this can increase the likelihood of structural failure compared with impacts at equal floor heights. Lastly, we note that several parameters were neglected in this study; for example, P-delta effect, soil-structure interaction, direction of incidence of earthquake and structural system. We recommend that additional studies are conducted to take these parameters into account.

## 8. Declarations

### 8.1. Author Contributions

Conceptualization, Y.J. and H.F.; methodology, Y.J.; software, Y.J.; validation, Y.J. and H.F.; formal analysis, Y.J.; investigation, Y.J.; resources, Y.J.; data curation, Y.J.; writing—original draft preparation, Y.J.; writing—review and editing, H.F.; visualization, Y.J.; supervision, H.F.; project administration, H.F.; funding acquisition, Y.J. and H.F. All authors have read and agreed to the published version of the manuscript.

### 8.2. Data Availability Statement

The data presented in this study are available in the article.

### 8.3. Funding

The authors received no financial support for the research, authorship, and/or publication of this article.

### 8.4. Conflicts of Interest

The authors declare no conflict of interest.

## 9. References

- [1] Zheng, Y., Xiao, X., Zhi, L., & Wang, G. (2015). Evaluation on impact interaction between abutment and steel girder subjected to nonuniform seismic excitation. *Shock and Vibration*, 2015. doi:10.1155/2015/981804.
- [2] Schramm, U., & Pilkey, W. D. (1996). Optimal design of structures under impact loading. *Shock and Vibration*, 3(1), 69-81. doi:10.3233/SAV-1996-3108.
- [3] Naderpour, H., Barros, R. C., Khatami, S. M., & Jankowski, R. (2016). Numerical Study on Pounding between Two Adjacent Buildings under Earthquake Excitation. *Shock and Vibration*, 2016, 1–9. doi:10.1155/2016/150478.
- [4] Anagnostopoulos, S. A. (1995, August). Earthquake induced pounding: State of the art. Proceedings of the 10<sup>th</sup> European Conference on Earthquake Engineering. 28 August-2 September, 1994, Rotterdam, Netherlands.
- [5] Anagnostopoulos, S. A. (1996). Building pounding re-examined: how serious a problem is it. 11<sup>th</sup> world conference on earthquake engineering, 23-28 June, 1996, Acapulco, Mexico.
- [6] Rosenblueth, E., & Meli, R. (1986). The 1985 Mexico Earthquake. *Concrete international*, 8(5), 23-34.
- [7] Valles-Mattox, R., & Reinhorn, A. (1996). Evaluation, prevention and mitigation of pounding effects in building structures. 11<sup>th</sup> world conference on earthquake engineering, 23-28 June, 1996, Acapulco, Mexico.
- [8] Lin, J., & Weng, C. (2002). A study on seismic pounding probability of buildings in Taipei metropolitan area. *Journal of the Chinese Institute of Engineers*, 25(2), 123–135. doi:10.1080/02533839.2002.9670687.
- [9] Lin, C. C. J., Hung, H. H., Liu, K. Y., & Chai, J. F. (2010). Reconnaissance observation on bridge damage caused by the 2008 Wenchuan (China) earthquake. *Earthquake Spectra*, 26(4), 1057–1083. doi:10.1193/1.3479947.
- [10] Cole, G., Chouw, N., & Dhakal, R. (2011). Building and bridge pounding damage observed in the 2011 Christchurch earthquake. *Bulletin of the New Zealand Society for Earthquake Engineering*, 44(4), 334–341. doi:10.5459/bnzsee.44.4.334-341.
- [11] Chouw, N., & Hao, H. (2012). Pounding damage to buildings and bridges in the 22 February 2011 Christchurch earthquake. *International Journal of Protective Structures*, 3(2), 123–140. doi:10.1260/2041-4196.3.2.123.
- [12] Shrestha, B., & Hao, H. (2018). Building Pounding Damages Observed during the 2015 Gorkha Earthquake. *Journal of Performance of Constructed Facilities*, 32(2), 4018006. doi:10.1061/(asce)cf.1943-5509.0001134.
- [13] Pratesi, F., Sorace, S., & Terenzi, G. (2014). Analysis and mitigation of seismic pounding of a slender R/C bell tower. *Engineering Structures*, 71, 23–34. doi:10.1016/j.engstruct.2014.04.006.
- [14] Liolios, A., Liolios, A., Hatzigeorgiou, G., & Radev, S. (2014). Pounding effects on the earthquake response of adjacent reinforced concrete structures strengthened by cable elements. *Journal of Theoretical and Applied Mechanics (Poland)*, 44(2), 41–56. doi:10.2478/jtam-2014-0009.
- [15] Kazemi, F., Miari, M., & Jankowski, R. (2021). Investigating the effects of structural pounding on the seismic performance of adjacent RC and steel MRFs. *Bulletin of Earthquake Engineering*, 19(1), 317–343. doi:10.1007/s10518-020-00985-y.
- [16] Filiatrault, A., Wagner, P., & Cherry, S. (1995). Analytical prediction of experimental building pounding. *Earthquake Engineering & Structural Dynamics*, 24(8), 1131–1154. doi:10.1002/eqe.4290240807.
- [17] Chau, K. T., Wei, X. X., Guo, X., & Shen, C. Y. (2003). Experimental and theoretical simulations of seismic poundings between two adjacent structures. *Earthquake Engineering and Structural Dynamics*, 32(4), 537–554. doi:10.1002/eqe.231.
- [18] Jaradat, Y., Sobhi, P., & Far, H. (2023). An Investigation into Adequacy of Separation Gap to Preclude Earthquake-induced Pounding. *Structural Engineering and Mechanics*.
- [19] Rahman, A. M., Carr, A. J., & Moss, P. J. (2000). Structural pounding of adjacent multi-storey structures considering soil flexibility effects. Proceedings of the 12<sup>th</sup> World Conference on Earthquake Engineering, 30 January, 2000, Auckland, New Zealand.
- [20] Chouw, N. (2002). Influence of soil-structure interaction on pounding response of adjacent buildings due to near-source earthquakes. *Journal of Applied Mechanics*, 5, 543–553. doi:10.2208/journalam.5.543.
- [21] Saleh, A., Far, H., & Mok, L. (2018). Effects of different support conditions on experimental bending strength of thin walled cold formed steel storage upright frames. *Journal of Constructional Steel Research*, 150, 1–6. doi:10.1016/j.jcsr.2018.07.031.

- [22] Hao, H., Bi, K., Chouw, N., & Ren, W. X. (2013). State-of-the-art review on seismic induced pounding response of bridge structures. *Journal of Earthquake and Tsunami*, 7(3), 1350019. doi:10.1142/S179343111350019X.
- [23] Jia, H. Y., Lan, X. L., Zheng, S. X., Li, L. P., & Liu, C. Q. (2019). Assessment on required separation length between adjacent bridge segments to avoid pounding. *Soil Dynamics and Earthquake Engineering*, 120, 398–407. doi:10.1016/j.soildyn.2019.01.031.
- [24] Cole, G., Dhakal, R., Carr, A., & Bull, D. (2010). Interbuilding pounding damage observed in the 2010 darfield earthquake. *Bulletin of the New Zealand Society for Earthquake Engineering*, 43(4), 382–386. doi:10.5459/bnzsee.43.4.382-386.
- [25] Maison, B. F., & Kasai, K. (1990). Analysis for a Type of Structural Pounding. *Journal of Structural Engineering*, 116(4), 957–977. doi:10.1061/(asce)0733-9445(1990)116:4(957).
- [26] Anagnostopoulos, S. A. (1988). Pounding of buildings in series during earthquakes. *Earthquake Engineering & Structural Dynamics*, 16(3), 443–456. doi:10.1002/eqe.4290160311.
- [27] Jankowski, R., Wilde, K., & Fujino, Y. (1998). Pounding of superstructure segments in isolated elevated bridge during earthquakes. *Earthquake Engineering and Structural Dynamics*, 27(5), 487–502. doi:10.1002/(SICI)1096-9845(199805)27:5<487::AID-EQE738>3.0.CO;2-M.
- [28] Anagnostopoulos, S. A., & Spiliopoulos, K. V. (1992). An investigation of earthquake induced pounding between adjacent buildings. *Earthquake Engineering & Structural Dynamics*, 21(4), 289–302. doi:10.1002/eqe.4290210402.
- [29] Crozet, V., Politopoulos, I., Yang, M., Martinez, J. M., & Erlicher, S. (2017). Influential Structural Parameters of Pounding between Buildings during Earthquakes. *Procedia Engineering*, 199, 1092–1097. doi:10.1016/j.proeng.2017.09.084.
- [30] Shehata E. Abdel Raheem. (2006). Seismic Pounding between Adjacent Building Structures. *Electronic Journal of Structural Engineering*, 6, 66–74. doi:10.56748/ejse.659.
- [31] Mate, N. U., Bakre, S. V., & Jaiswal, O. R. (2012). Comparative study of impact simulation models for linear elastic structures in seismic pounding. 15<sup>th</sup> World Conference on Earthquake Engineering, 24–28 September, 2012, Lisbon, Portugal.
- [32] Muthukumar, S., & DesRoches, R. (2006). A Hertz contact model with non-linear damping for pounding simulation. *Earthquake Engineering and Structural Dynamics*, 35(7), 811–828. doi:10.1002/eqe.557.
- [33] Ye, K., Li, L., & Zhu, H. (2009). A note on the Hertz contact model with nonlinear damping for pounding simulation. *Earthquake Engineering and Structural Dynamics*, 38(9), 1135–1142. doi:10.1002/eqe.883.
- [34] Jankowski, R. (2005). Non-linear viscoelastic modelling of earthquake-induced structural pounding. *Earthquake Engineering and Structural Dynamics*, 34(6), 595–611. doi:10.1002/eqe.434.
- [35] Khatiwada, S., Chouw, N., & Butterworth, J. W. (2013). Evaluation of numerical pounding models with experimental validation. *Bulletin of the New Zealand Society for Earthquake Engineering*, 46(3), 117–130. doi:10.5459/bnzsee.46.3.117-130.
- [36] Pant, D. R., Wijeyewickrema, A. C., & Ohmachi, T. (2010). Seismic pounding between reinforced concrete buildings: A study using two recently proposed contact element models 14<sup>th</sup> European Conference on. *Earthquake Engineering*, 30 August-3 September, 2010, Ohrid, Republic of Macedonia.
- [37] Jaradat, Y., Far, H., & Mortazavi, M. (2022). Experimental Evaluation of Theoretical Impact Models for Seismic Pounding. *Journal of Earthquake Engineering*, 1–21. doi:10.1080/13632469.2022.2131654.
- [38] Goldsmith, W. (2001). *IMPACT—the theory and physics of colliding solids*. Dover Publication, New York, United States.
- [39] Komodromos, P., Polycarpou, P. C., Papaloizou, L., & Phocas, M. C. (2007). Response of seismically isolated buildings considering poundings. *Earthquake Engineering and Structural Dynamics*, 36(12), 1605–1622. doi:10.1002/eqe.692.
- [40] Licari, M., Sorace, S., & Terenzi, G. (2015). Nonlinear modeling and mitigation of seismic pounding between R/C frame buildings. *Journal of Earthquake Engineering*, 19(3), 431–460. doi:10.1080/13632469.2014.984370.
- [41] Guo, A., Cui, L., & Li, H. (2012). Impact stiffness of the contact-element models for the pounding analysis of highway bridges: Experimental evaluation. *Journal of Earthquake Engineering*, 16(8), 1132–1160. doi:10.1080/13632469.2012.693243.
- [42] Wada, A., Shinozaki, Y., & Nakamura, N. (1984). Collapse of building with expansion joints through collision caused by earthquake motion. *Proceedings of the 8<sup>th</sup> World Conference on Earthquake Engineering*, 21–28 July, 1984, San Francisco, United States.
- [43] Maison, B. F., & Kasai, K. (1992). Dynamics of pounding when two buildings collide. *Earthquake Engineering & Structural Dynamics*, 21(9), 771–786. doi:10.1002/eqe.4290210903.
- [44] Jankowski, R. (2008). Comparison of Numerical Models of Impact Force for Simulation of Earthquake-Induced Structural Pounding. *Lecture Notes in Computer Science*, 710–717. doi:10.1007/978-3-540-69384-0\_76.

- [45] Cole, G. L., Dhakal, R. P., Carr, A. J., & Bull, D. K. (2012). 3D modelling of building pounding including diaphragm flexibility. 15<sup>th</sup> World Conference on Earthquake Engineering, 24–28 September, 2012, Lisbon, Portugal.
- [46] Jaradat, Y., & Far, H. (2021). Optimum stiffness values for impact element models to determine pounding forces between adjacent buildings. *Structural Engineering and Mechanics*, 77(2), 293–304. doi:10.12989/sem.2021.77.2.293.
- [47] Cole, G., Dhakal, R., Carr, A., & Bull, D. (2011). An investigation of the effects of mass distribution on pounding structures. *Earthquake Engineering and Structural Dynamics*, 40(6), 641–659. doi:10.1002/eqe.1052.
- [48] Xu, X., Xu, X., Liu, W., & Zhou, D. (2016). A new formula of impact stiffness in linear viscoelastic model for pounding simulation. *Shock and Vibration*, 2016. doi:10.1155/2016/5861739.
- [49] Ghandil, M., & Aldaikh, H. (2017). Damage-based seismic planar pounding analysis of adjacent symmetric buildings considering inelastic structure–soil–structure interaction. *Earthquake Engineering and Structural Dynamics*, 46(7), 1141–1159. doi:10.1002/eqe.2848.
- [50] Naserkhaki, S., Aziz, F. N. A. A., & Pourmohammad, H. (2012). Parametric study on earthquake induced pounding between adjacent buildings. *Structural Engineering and Mechanics*, 43(4), 503–526. doi:10.12989/sem.2012.43.4.503.
- [51] López-Almansa, F., & Kharazian, A. (2018). New formulation for estimating the damping parameter of the Kelvin-Voigt model for seismic pounding simulation. *Engineering Structures*, 175, 284–295. doi:10.1016/j.engstruct.2018.08.024.
- [52] Polycarpou, P. C., & Komodromos, P. (2010). Earthquake-induced poundings of a seismically isolated building with adjacent structures. *Engineering Structures*, 32(7), 1937–1951. doi:10.1016/j.engstruct.2010.03.011.
- [53] Abdel-Mooty, M., Al-Atrpy, H., & Ghounaim, M. (2009). Modeling and analysis of factors affecting seismic pounding of adjacent multi-story buildings. *Earthquake Resistant Engineering Structures VII*. doi:10.2495/eres090121.
- [54] Tabatabaiefar, S., Fatahi, B., & Samali, B. (2014). Numerical and experimental investigations on seismic response of building frames under influence of soil-structure interaction. *Advances in Structural Engineering*, 17(1), 109–130. doi:10.1260/1369-4332.17.1.109.
- [55] Chopra, A. K. (2007). *Dynamics of structures*. Pearson Education India, Noida, India.
- [56] Papagiannopoulos, G. A., & Hatzigeorgiou, G. D. (2011). On the use of the half-power bandwidth method to estimate damping in building structures. *Soil Dynamics and Earthquake Engineering*, 31(7), 1075–1079. doi:10.1016/j.soildyn.2011.02.007.
- [57] Tabatabaiefar, H. R. (2016). Detail design and construction procedure of laminar soil containers for experimental shaking table tests. *International Journal of Geotechnical Engineering*, 10(4), 328–336. doi:10.1080/19386362.2016.1145419.
- [58] Yaghmaei-Sabegh, S., & Jalali-Milani, N. (2012). Pounding force response spectrum for near-field and far-field earthquakes. *Scientia Iranica*, 19(5), 1236–1250. doi:10.1016/j.scient.2012.07.012.
- [59] Hatzigeorgiou, G. D. (2010). Damping modification factors for SDOF systems subjected to near-fault, far-fault and artificial earthquakes. *Earthquake Engineering and Structural Dynamics*, 39(11), 1239–1258. doi:10.1002/eqe.991.
- [60] Yaghmaei-Sabegh, S., & Tsang, H. H. (2011). An updated study on near-fault ground motions of the 1978 Tabas, Iran, earthquake ( $M_w = 7.4$ ). *Scientia Iranica*, 18(4 A), 895–905. doi:10.1016/j.scient.2011.07.018.
- [61] K-Karamodin, A., & H-Kazemi, H. (2010). Semi-active control of structures using neuro-predictive algorithm for MR dampers. *Structural Control and Health Monitoring*, 17(3), 237–253. doi:10.1002/stc.278.
- [62] Singh, V., & Sangle, K. (2022). Analysis of vertically oriented coupled shear wall interconnected with coupling beams. *HighTech and Innovation Journal*, 3(2), 230-242. doi:10.28991/HIJ-2022-03-02-010.
- [63] Ptilakis, D., Dietz, M., Wood, D. M., Clouteau, D., & Modaressi, A. (2008). Numerical simulation of dynamic soil-structure interaction in shaking table testing. *Soil Dynamics and Earthquake Engineering*, 28(6), 453–467. doi:10.1016/j.soildyn.2007.07.011.
- [64] AS/NZS3678. (2011). *Structural steel—Hot-rolled plates, floorplates and slabs*. Australian Standards, Sydney, Australia.
- [65] Naserkhaki, S., El-Richa, M., Abdul Azizb, F. N. A., & Pourmohammadc, H. (2013). Separation gap, a critical factor in earthquake induced pounding between adjacent buildings. *Asian Journal of Civil Engineering*, 14(6), 881–898.
- [66] Bennett, J. O., Briggs, W. L., & Badalamenti, A. (2008). *Using and understanding mathematics: A quantitative reasoning approach*. Pearson Addison Wesley, Reading, United Kingdom.
- [67] Far, H., & Flint, D. (2017). Significance of using isolated footing technique for residential construction on expansive soils. *Frontiers of Structural and Civil Engineering*, 11(1), 123–129. doi:10.1007/s11709-016-0372-8.